Insights into the viscohyperelastic response of soft magnetorheological elastomers: Competition of macrostructural versus microstructural players

S. Lucarini, M.A. Moreno-Mateos, K. Danas, D. Garcia-Gonzalez

Insights into the viscohyperelastic response of soft magnetorheological elastomers: competition of macrostructural versus microstructural players

S. Lucarini[a], M.A. Moreno-Mateos[a], K. Danas[b], D. Garcia-Gonzalez[a,*]

[a] *Department of Continuum Mechanics and Structural Analysis, University Carlos III of Madrid, Avda. de la Universidad 30, 28911 Leganés, Madrid, Spain*
[b] *LMS, C.N.R.S, École Polytechnique, Institut Polytechnique de Paris, Palaiseau, 91128, France*

Abstract

Magnetorheological elastomers (MREs) are multifunctional composites that consist of an elastomeric matrix filled with magnetic particles. These materials respond to an external magnetic field by mechanically deforming and/or changing their magnetorheological properties. Such a multi-physical response has made them extraordinary candidates for a wide variety of applications in soft robotics and bioengineering. However, there are still some gaps of knowledge that prevent the optimal design and application of these MREs. In this regard, the effect of viscoelastic mechanisms remains elusive from a microstructural perspective. To the best of the authors' knowledge, this work provides for the first time a numerical homogenization analysis for various magneto-active microstructures accounting for viscous deformation mechanisms. To this end, we propose an incremental variational formulation that incorporates viscoelasticity via internal variables, which is properly modified to deal with the continuity of Maxwell stresses. The proposed framework is applied to study the magneto-mechanical couplings in extremely soft MREs (stiffness < 10 kPa). Such soft matrix promotes microstructural rearrangements while transmitting internal forces leading to macrostructural synergistic responses. The constitutive parameters are calibrated with experimental tests taken from a previous work by the authors. The numerical results are accompanied with original magnetostriction tests considering different sample geometries and confined magneto-mechanical tests, reporting the macroscopic response. The results obtained in this work suggest that the effective magneto-mechanical response of the MRE is the outcome of a com-

*Corresponding author
Email address: danigarc@ing.uc3m.es (D. Garcia-Gonzalez)

petition between macrostructural and local microstructural responses, where viscous mechanisms play a relevant role.

Keywords: Magnetorheological elastomer (MRE), Constitutive modeling, Multifunctional composites, Viscoelasticity, Microstructural Homogenization

1. Introduction

Magnetorheological elastomers (MREs) are multifunctional composites that consist of an elastomeric matrix filled with magnetic particles. The MREs respond to magnetic fields offering possibilities of remote and reversible stimulation [1, 2, 3]. This allows for varying their mechanical properties, such as the stiffness, the natural frequency, or the damping capacity, which can significantly change when subjected to external magnetic fields [4, 5]. The magnetic fillers contained within the composite are responsible for their magnetostrictive response (mechanical deformation under applied magnetic fields) [6, 7]. Among the rather general class of MREs, magnetically and mechanically soft responsive materials or soft MREs[1] have become a subject of interest in recent years due to the wide range of applications in soft robotics, bio-medicine or industrial components [8, 9, 10, 11]. These stimuli-responsive *smart* materials enable untethered, fast, and reversible actuation and/or changes in mechanical properties. MREs can be manufactured by embedding magnetizable particles into highly compliant matrices (stiffness below 100 kPa) [12, 13]. Compared to conventional stiffer MREs, the response of these mechanically and magnetically soft MREs can be governed by different magnetic actuation mechanisms. The soft and compliant matrix allows for large deformations when external environmental forces and magnetic stimuli are applied, which facilitates potential rearrangements of particles [14, 15, 16].

A comprehensive characterization of the MREs is indispensable to understand their exceptional behavior [17, 18]. Regarding the experimental works investigating their magneto-mechanical behavior, seminal publications were focused on the change of properties, i.e., Young's modulus [2, 19, 20]. Regarding the viscoelastic properties of MREs, some experimental works measured their storage

[1] We would like to note that henceforth the word "soft" will be used to insist on the mechanically very soft response of the MRE materials, while the magnetic response is also soft, ie., does not exhibit any magnetic dissipation.

and loss moduli when subjected to tensile, compression or shear deformation modes under the application of external magnetic fields [21, 22, 23, 24]. However, the magnetostrictive response of the soft MREs (below 100 kPa) is extremely complex since, depending on the experimental conditions such as sample geometry or test conditions, they can show either compressive [25, 26] or expansive [27] behaviors when applying magnetic fields. Moreover, when composed of viscous compliant matrices, they also provide an unusual time-dependent response [27, 28]. This complex behavior can only be explained by microscopic particle interactions in combination with macroscopic effects. Thus, careful modeling studies are needed to understand the coupled magneto-mechanical behavior occurring at the microscale and its effect by scaling up to the macroscale level.

The mathematical modeling of the coupled mechanical and magnetic effects in MREs has been addressed by different modeling approaches [29, 30]. From a macroscopic point of view, the composite can be considered as a homogeneous continuum. This enables the representation of real structures under complex loading conditions with a reasonable computational effort, where effects of the underlying microstructure are captured implicitly via magneto-mechanical coupling terms [31, 32, 33, 34, 35]. Regarding the modeling of the magneto-visco-elastic coupled behavior of MREs, based on Dorfmann and Ogden's formulation [32], Saxena et al. [36] proposed a formulation for finite deformation magneto-viscoelasticity. This work considers dissipation due to mechanical viscoelasticity of the polymeric matrix and the resistance of the material to overall magnetization. These continuum models can phenomenologically capture the magneto-visco-elastic coupling but do not account explicitly for microstructural features. From a microscopic point of view, two main approaches can be differentiated: particle interaction (or lattice based) and full-field homogenization models. Particle interaction models were presented in previous works [37, 38, 39, 40], which are based on magneto-mechanical energy minimization taking the assumption that the magnetizable particles behave as dipoles. These incorporate microstructural information, but do not account for the heterogeneities in the magnetic field that appear as a function of the particles distributions as well as long range interactions between particles. Garcia-Gonzalez and Hossain [41] extended this approach to consider viscoelasticity and predict relaxation responses in soft MREs, and later in hard magnetic MREs [42]. However, these lattice-based models, albeit extremely useful since they

are explicit in nature, present limitations such as the modeling of particles-matrix interactions in heterogeneous spatial distributions of particles, spatial fluctuations of magnetic fields within the MRE, and limitations in the nature of the modeled dipole-dipole interactions.

Another microstructural approach is the homogenization of the magneto-mechanical problem. This approach is divided into full-field numerical approaches [43, 44, 45, 46, 47, 48, 49, 50] and analytical ones in two dimensions [51, 52] and in three dimensions [53, 54, 49, 55]. The full-field numerical modeling naturally accounts for microstructural features such as magnetic particle distributions and interactions with the matrix phase but tends to be extremely time consuming especially if more realistic random microstructures are considered. The analytical models usually describe the interactions in an average manner and thus do not provide insight into the local micro-deformation mechanisms. Yet, they are extremely powerful when those are explicit since they can be used to analyze complex non-linear magneto-mechanical Boundary Value Problems (BVPs) by their proper implementation in general purpose Finite Element Method (FEM) software [56]. Despite the great potential of the previously-mentioned homogenization full-field models, to the best of the authors' knowledge, there are no homogenization frameworks accounting for the viscous behavior of the matrix and nor applications for extremely soft MREs (below 10 kPa), save for a very recent study in the purely mechanical context [57]. Therefore, the role of the microstructure in such a coupled regime is still an open problem, and some aspects related to viscous deformation mechanisms need further investigation.

This work aims at understanding the role of viscous deformation mechanisms at the microstructural level and how these are scaled up to govern the magneto-mechanical macroscopic response of extremely soft MREs (polymeric matrix $\approx$ 1 kPa). To this end, we have developed a full-field numerical homogenization framework to naturally capture the effects of external magnetic fields on the nonlinear viscoelastic behavior of these composites. To the authors' knowledge, this is the first homogenization framework for the study of the magneto-viscous-mechanical problem in such extremely soft MREs, whose mechanical response can be activated with relatively low magnetic fields (below 50-100 mT). To motivate and calibrate the model, we make use of recently published experimental data [27] and provide further original experiments. After validation of the mechanical

part of the model, we use it to explore viscous responses under external magnetic fields for different particle arrangements within the MRE. Finally, we provide ad-hoc simulations to propose a link between microstructural arrangements and macroscopic responses observed experimentally. Overall, this work suggests that a competition between macrostructural and local microstructural responses governs the effective magneto-mechanical response of the MRE, and that viscous mechanisms play a relevant role in the deformation process.

2. Magnetorheological response at the macroscale: experimental insights

This section provides experimental tests on MREs to provide a clear picture of the effective macroscopic response of the MREs under the application of an external magnetic field. The baseline materials chosen for the manufacturing are an elastomeric component for the matrix phase and soft magnetic particles. The elastomeric matrix is made of Dowsil CY52-276 (DowSil, Midland, MI, USA) (PDMS). The magnetic particles are made of soft SQ carbonyl iron powder (CIP) (BASF, Germany) with an average diameter of 3.9–5.0 μm. For the manufacturing of the samples, we followed the methodology presented in a previous work [27]. Note that cylindrical samples of 1mm height and 20 mm diameter are used to ensure homogeneous magnetic fields within the testing region (i.e., homogeneous fields in the vacuum with all the field lines following the same direction and magnitude, see further details in [27]). In addition, monotonous compression curves were piked from [27] to calibrate and validate the homogenization model.

2.1. Macroscopic magnetic characterization

The experiments provided in this section aim at studying the mechanical response of MREs under external magnetic fields. To this end, two types of experiments are considered: i) free mechanical expansion tests under axial magnetic fields; ii) axially confined tests under axial magnetic fields. The MRE specimen is placed between flat plates composed of austenitic stainless steel (with relative magnetic permeability close to 1). Bellow the specimen, a coil system generates the requested magnetic field aligned in the axial direction of the specimen. Note that we use a close loop system

where the temperature is constantly regulated as well as the magnetic field by the use of a thermocouple and a hall probe, respectively. More detail about the experimental setup can be found in [27].

The first set of experiments consists in cylindrical specimens of different particle volume fractions $\phi = \{0, 0.1, 0.2, 0.3\}$ and diameters $D = \{4, 6, 20\}$ mm (experiments for 6 and 20 mm are originally performed in this work as an extension of those for 4 mm in [27]) that are subjected to axial magnetic fields under free boundary conditions. Under the application of an external magnetic field, the specimen undergoes magnetic interactions between particles and with the external field leading to internal forces in the composite. As a consequence, the MRE experiences mechanical deformation and shape changes. To allow for the visualization of the MREs' deformation process, we performed these experiments without using the metallic cover that ensures a spatially homogeneous magnetic field in the whole specimen region. To evaluate the influence of such heterogeneity in the magnetic field, we reduced the specimen diameter up to 4 mm, where the magnetic field was measured to be homogeneous. In addition, we conducted these tests with and without the presence of the upper plate. These tests allow for identifying potential boundary effects due to a possible magnetization of the plate. These results are all collected together in Figure 1.

A first important observation is that all the MREs tested macroscopically expand instead of contracting. It can be observed that such an expansion along the axial direction, here aligned with the magnetic field, is directly related to the particle volume fraction. In this regard, higher deformations are obtained when increasing the particle content (Figure 1). Another important feature is the homogeneity of the deformation state in the small samples. However, a highly heterogeneous deformation is shown for the samples with the highest diameter. In these tests, the magnetic field reaches maximum values in the center of the specimen and a macrostructural response governs the deformation of its peripheral regions, i.e., these outer domains tend to macroscopically align with the central axial magnetic lines. Finally, it is important to note that the same observations have been obtained for tests without the presence of the upper plate (Figure 1). These results discard a potential magnetization effect of the upper plate acting as a magnetic pole attracting the particles. Therefore, it can be concluded that the MREs tested under an axial magnetic field

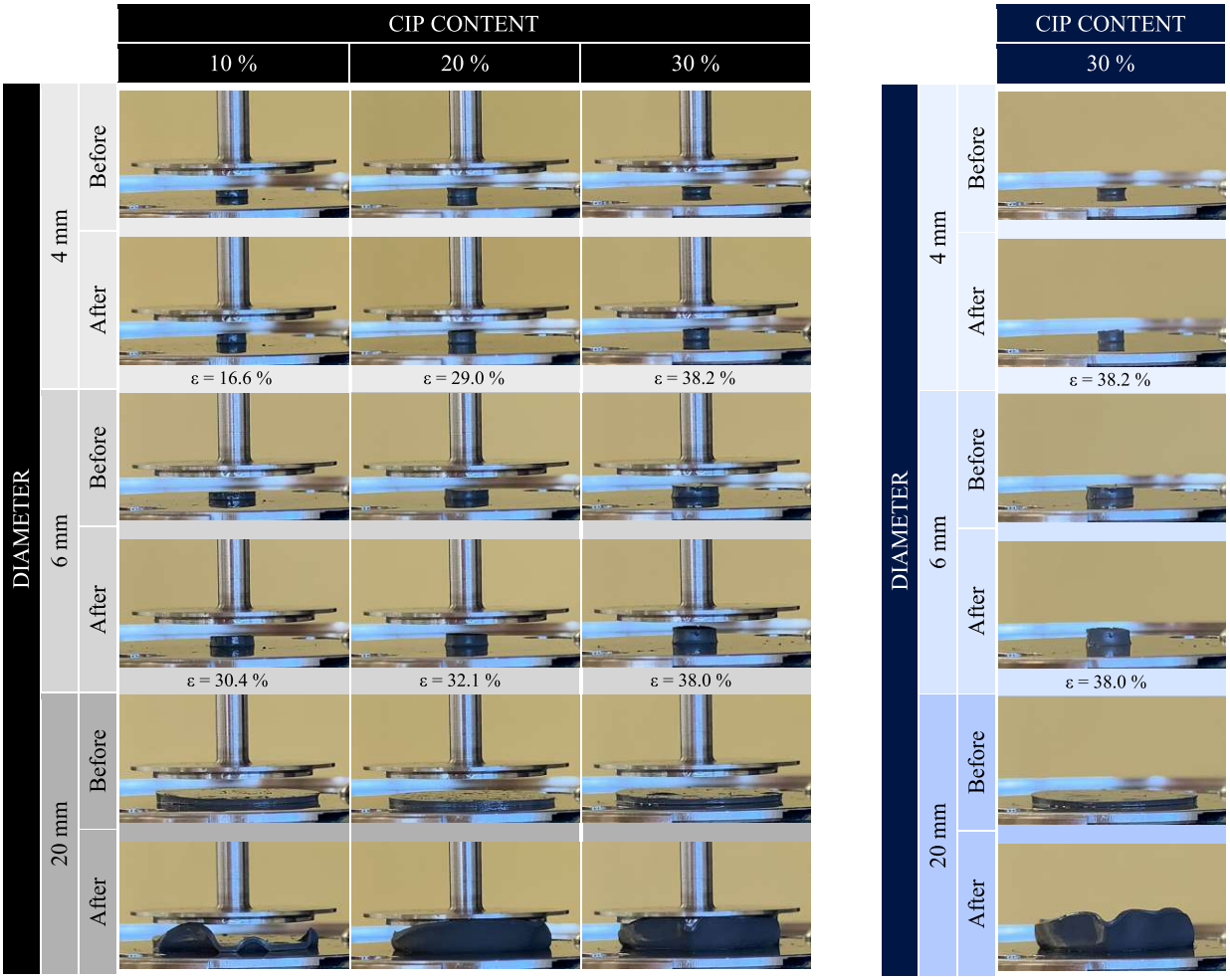

Figure 1: Mechanical response of MREs under the application of an external magnetic field for different particles volume fractions $\phi = \{0, 0.1, 0.2, 0.3\}$ and diameters $D = \{4, 6, 20\}$ mm. Note that the test for 4 mm specimens was picked from [27] and have been extended for other geometries to explore the macroscopic response of extremely soft MREs. The right hand side table shows the exact same tests for $\phi = 0.3$ without the presence of the upper plate. All the specimens were prepared with an initial height of 1 mm. The magnetic field was imposed in the form of a temporal ramp until reaching a maximum value of 0.25 T.

respond macroscopically by expanding in such a direction.

The second set of experiments considers cylindrical specimens of different particle volume fractions $\phi = \{0, 0.1, 0.2, 0.3\}$ and a fixed geometry of 1 mm height and 20 mm diameter, that are subjected to axial magnetic fields under axially confined mechanical boundary conditions. These tests aim at providing a quantitative analysis of the forces experienced within the MREs due to the application of the external magnetic field at different rates. To this end, the experimental setup is such that ensures homogeneous magnetic field conditions within the whole specimen region. During the tests,

the magnetic field is imposed in the form of a temporal ramp while keeping the upper plate fixed at the initial height of the specimen. Thus, the force exerted by the MRE due to the magnetorheological response is tracked by the load cell of the equipment. The mean curves calculated from the results of six specimens are shown in Figure 2. All the specimens present a parabolic response with axial force (directly related to internal MRE magnetic stress) increasing for larger magnetic inductions. The magnitude of the axial force exerted on the upper plate increases with the content of magnetic particles. Finally, we noted that different magnetic field application rates do not result in different experimental curves (these were almost superimposed). This interesting point can be explained by the fact that when the magnetic field is applied, interaction forces between particles and the external field are generated. Thus, the particles try to rearrange to find the new equilibrium state. However, the elastomeric matrix opposes this rearrangement, balancing the related magnetic stress by mechanical deformation. Hence, the axial force measured at the upper plate is related to the mechanical stress experienced by the matrix that, despite its viscoelastic nature, is driven by the generated magnetic stress. Therefore, although viscous relaxation processes are happening within the elastomeric phase, these are not observed at the macroscopic response in these tests. This point will be revisited in the following sections making use of a microstructural computational framework.

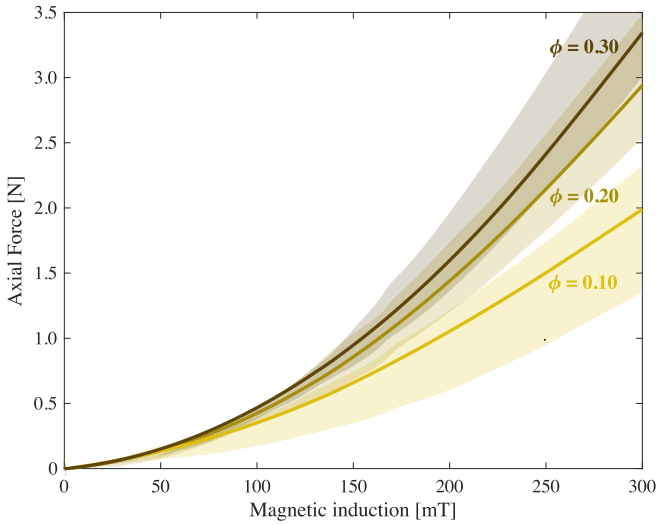

Figure 2: Experimental results for the axially confined tests under axial magnetic fields on cylindrical specimens of 1 mm height and 20 mm diameter. Axial force measured by the load cell of the test machine is plotted versus magnetic induction for three magnetic particle volume fractions $\phi = \{0.1, 0.2, 0.3\}$. The magnetic field is applied at constant rates from 0.2 to 20 mT/s. Note that the magnetic application rates imposed in these tests provided almost superimposed results without significant differences in their mean curve. These results are equivalent to those presented in [27], but covering a broader range of magnetic rates.

3. Microstructural constitutive framework for magneto-viscoelasticity

This section introduces the formulation used to describe the microstructural response of soft ($\approx$ 1 kPa) MREs subjected to different combinations of magneto-mechanical loading conditions. In the following, we present the kinematics of the framework, the balance equations and thermodynamics and, then, we specialize the constitutive definitions and describe the homogenization approach.

3.1. Kinematics and balance equations

The microstructural modeling is intended to shed light on the understanding of the magnetically induced deformation mechanisms and the interaction with the visco-elastic behavior of the matrix in the context of magnetic particle filled MREs. The extremely soft nature of the polymeric material employed as matrix makes these MREs highly deformable. Therefore, it is customary to frame the modeling in finite deformations differentiating between the material configuration Ω_0 and the spatial configuration Ω. The primary fields involved in this problem are the displacement field $\mathbf{u}(\mathbf{x})$ and a magnetic scalar potential $\phi(\mathbf{x})$, whose gradients in the reference configuration yield

the deformation gradient $\mathbf{F}(\mathbf{x})$ and the Lagrangian magnetic field $\mathbf{H}(\mathbf{x})$, such that

$$\mathbf{F}(\mathbf{x}) = \mathbf{I} + \nabla_0 \mathbf{u}(\mathbf{x}) \quad \text{and} \quad \mathbf{H}(\mathbf{x}) = -\nabla_0 \phi(\mathbf{x}). \tag{1}$$

Here, $\mathbf{I}$ is the second-order identity tensor.

To account for time-dependent responses associated to the viscoelastic nature of the polymeric phase and the related relaxation mechanisms and dissipation effects, an iso-strain model is used with one viscous branch. The isochoric deformation gradient is further decomposed into elastic ($\mathbf{F}_e$) and viscous ($\mathbf{F}_v$) components as

$$\mathbf{F} = \mathbf{F}_e \cdot \mathbf{F}_v, \tag{2}$$

where the viscous component $\mathbf{F}_v$ is considered as state variable.

Along with the previous fields, we account also for two fundamental magnetic variables; the Lagrangian magnetic field $\mathbf{H}$, and the Lagrangian magnetic induction $\mathbf{B}$. These can be expressed, alternatively, in their Eulerian forms as

$$\mathbf{h} = \mathbf{H} \cdot \mathbf{F}^{-1}, \quad \mathbf{b} = J^{-1}\mathbf{F} \cdot \mathbf{B}, \tag{3}$$

where $J = \det(\mathbf{F})$. The Eulerian (current) magnetization $\mathbf{m}$ can be obtained from the following constitutive relation

$$\mathbf{m} = \frac{\mathbf{b}}{\mu_0} - \mathbf{h}, \tag{4}$$

where μ_0 is the magnetic permeability of free space. Regarding the governing equations, the mechanical balance, in the material configuration and in the absence of body forces, can be written as

$$\nabla_0 \cdot \mathbf{P} = \mathbf{0}, \tag{5}$$

where $\mathbf{P}$ is the first Piola-Kirchhoff stress tensor. Note that inertial terms are neglected in this work. The influence of these was evaluated by conducting an experiment where we exposed the soft MRE to a set of permanent magnets approaching fast to it. The viscosity of the polymeric phase was observed to rule the overall response of the MRE leading to negligible dynamic oscillations

of the sample (nor local neither global). However, this is an interesting question that must be carefully addressed in future works analyzing the implications of micro-inertial terms within the MRE depending on the polymeric matrix used.

Moreover, the magnetic problem considers the Maxwell's equations for magneto-statics that, in the material configuration, are defined as

$$\nabla_0 \times \mathbf{H} = \mathbf{0}, \quad \nabla_0 \cdot \mathbf{B} = 0. \tag{6}$$

3.2. Thermodynamics

Considering isothermal conditions, we define an energy density function that depends on the deformation gradient $\mathbf{F}$, the magnetic field $\mathbf{H}$, and the internal variables, i.e., the viscous deformation gradient $\mathbf{F}_v$, as $\Psi(\mathbf{F}, \mathbf{H}, \mathbf{F}_v)$. Considering the incompressibility condition for MREs under study, the second law of thermodynamics in the form of Clausius-Duhem inequality becomes

$$\mathbf{P} : \dot{\mathbf{F}} + pJ\mathbf{F}^{-T} : \dot{\mathbf{F}} - \mathbf{B} \cdot \dot{\mathbf{H}} - \frac{\partial \Psi}{\partial \mathbf{F}} : \dot{\mathbf{F}} - \frac{\partial \Psi}{\partial \mathbf{H}} \cdot \dot{\mathbf{H}} - \frac{\partial \Psi}{\partial \mathbf{F}_v} : \dot{\mathbf{F}}_v \geq 0, \tag{7}$$

where the term related to p (the Lagrange multiplier associated to the pressure) has been included to impose incompressibility. The constitutive equations can be consistently derived, applying the Coleman-Noll framework as

$$\mathbf{P} = \frac{\partial \Psi}{\partial \mathbf{F}} - pJ\mathbf{F}^{-T}, \quad \mathbf{B} = -\frac{\partial \Psi}{\partial \mathbf{H}}. \tag{8}$$

The remaining term associated to the internal variable $-\frac{\partial \Psi}{\partial \mathbf{F}_v} : \dot{\mathbf{F}}_v \geq 0$, establishes the consistency conditions allowing to define the evolution of such internal variable.

3.3. Local constitutive equations for constituents

This section specializes the constitutive relationships that describe the magneto-mechanical response of the microstructural constituents, i.e., polymeric matrix and magnetic particles.

3.3.1. Free energy functions and mechanical stress tensors

The constitutive behavior at a local point, for the matrix and the particles, is defined by the energy density function Ψ to account for mechanical and magnetic responses. Following standard knowledge of such materials, we consider both the polymer matrix and particle phases as incompressible[2]. In this work, the energy density is decomposed into three contributions, namely the mechanical energy, Maxwell energy and magnetization energy as

$$\Psi\left(\mathbf{F},\mathbf{H},\mathbf{F}_v\right)=\Psi_{mech}\left(\mathbf{F},\mathbf{F}_v\right)+\Psi_{maxw}\left(\mathbf{F},\mathbf{H}\right)+\Psi_{mag}\left(\mathbf{F},\mathbf{H}\right). \tag{9}$$

These energy density relations are posed to fulfill the material properties under study. The mechanical energy density follows a visco-hyperelastic model and can be further decomposed into elastic and viscous contributions along with a volumetric constraint

$$\Psi_{mech}\left(\mathbf{F},\mathbf{F}_v\right)=\begin{cases}\Psi^e_{mech}\left(\mathbf{F}\right)+\Psi^v_{mech}\left(\mathbf{F},\mathbf{F}_v\right) & \text{if} \quad J=1\\ +\infty, \quad \text{otherwise.}\end{cases} \tag{10}$$

We note at this point that the incompressibility constraint will be dealt with in the Section 3.4, where the incremental homogenization framework is described.

The elastic and viscous energetic contributions are defined following a Neo-Hookean formulation as

$$\begin{aligned}\Psi^e_{mech}\left(\mathbf{F}\right)&=\frac{\mu}{2}\left(I_1^{\mathbf{F}}-3\right),\\ \Psi^v_{mech}\left(\mathbf{F},\mathbf{F}_v\right)&=\frac{\mu_v}{2}\left(I_1^{\mathbf{F}_e}-3\right),\end{aligned} \tag{11}$$

with $I_1^{\mathbf{F}}=\mathrm{Tr}\left(\mathbf{F}\cdot\mathbf{F}^T\right)$ and $I_1^{\mathbf{F}_e}=\mathrm{Tr}\left(\mathbf{F}_e\cdot\mathbf{F}_e^T\right)$. The model parameters μ and μ_v represent the elastic and viscous shear moduli of the phase, respectively. From this energetic definition, the

[2]In reality, the particles exhibit a finite bulk modulus. Nonetheless, given their very large stiffness compared to that of the polymer, the effect of the actual value of the bulk modulus is of little importance provided that it is much larger than that of the matrix as is their shear modulus. This simplifies the numerical implementations.

mechanical part of the first Piola-Kirchhoff stress can be derived as

$$\mathbf{P}_{mech}\left(\mathbf{F},\mathbf{F}_v,p\right)=\frac{\partial\Psi_{mech}}{\partial\mathbf{F}}-p\mathbf{F}^{-T}, \tag{12}$$

where the term arising from incompressibility (addressed in Section 3.4) has been incorporated into this definition. Regarding the magnetic contributions, the background Maxwell energy in its standard expression for the material configuration reads as

$$\Psi_{maxw}\left(\mathbf{F},\mathbf{H}\right)=-\frac{\mu_0}{2}I_5^{\mathbf{H}} \tag{13}$$

where $I_5^{\mathbf{H}}=\left(\mathbf{F}^{-T}\cdot\mathbf{H}\right)\cdot\left(\mathbf{F}^{-T}\cdot\mathbf{H}\right)$ and the term J has been removed due to the incompressibility assumption. Moreover, the magnetization is accounted for by the hyperbolic tangent type magnetization relation described from the magnetic energy density function that reads, in the reference configuration, as

$$\Psi_{mag}\left(\mathbf{F},\mathbf{H}\right)=-\mu_0\left[\frac{m_s^2}{\chi}\log\left(\cosh\left(\frac{\chi}{m_s}\sqrt{I_5^{\mathbf{H}}}\right)\right)\right]. \tag{14}$$

Here, χ is the magnetic susceptibility and m_s is the magnetic saturation of the magnetization curve of the corresponding phase.

Then, the definition of the total first Piola-Kirchhoff stress can be derived from the total energy density by adding the magnetic components to the mechanical one, i.e.,

$$\mathbf{P}\left(\mathbf{F},\mathbf{H},\mathbf{F}_v\right)=\frac{\partial\Psi}{\partial\mathbf{F}}=\mathbf{P}_{mech}\left(\mathbf{F},\mathbf{F}_v\right)-\frac{\mu_0}{2}\frac{\partial I_5^{\mathbf{H}}}{\partial\mathbf{F}}-\mu_0\frac{m_s}{2\sqrt{I_5^{\mathbf{H}}}}\tanh\left(\frac{\chi}{m_s}\sqrt{I_5^{\mathbf{H}}}\right)\frac{\partial I_5^{\mathbf{H}}}{\partial\mathbf{F}} \tag{15}$$

with $\frac{\partial I_5^{\mathbf{H}}}{\partial\mathbf{F}}=-2\ \left(\mathbf{F}^{-T}\cdot\mathbf{H}\right)\otimes\left[\left(\mathbf{H}\cdot\mathbf{F}^{-1}\right)\cdot\mathbf{F}^{-T}\right]$. Notice that in Eq. (15), the terms of the partial derivatives arising form Maxwell and magnetization energy density functions appear, leading to magnetically induced forces.

Remark. It is noted here that the choice of the energy functions leads to an uncoupled magneto-mechanical response for each phase, i.e., the matrix and the particle (see a more detailed discussion in [47, 49]). The resulting magneto-mechanical coupling is an outcome of the complex interactions

between the particles and their rearrangements subject to the mechanical constraints imposed by the surrounding matrix phase. The Maxwell energy in the otherwise non-magnetic matrix phase serves to describe the background magnetic energy due to the presence of a non-zero magnetic permeability, that of vacuum.

3.3.2. Magnetic constitutive equation

In a similar fashion and making use of Eq. (8), the resulting definition of the magnetic flux as a function of the magnetic field yields into

$$\mathbf{B}\left(\mathbf{F},\mathbf{H}\right)=-\frac{\partial\Psi}{\partial\mathbf{H}}=\mu_0\left[1+\frac{m_s}{\sqrt{I_5^{\mathbf{H}}}}\tanh\left(\frac{\chi}{m_s}\sqrt{I_5^{\mathbf{H}}}\right)\right]\mathbf{F}^{-1}\cdot\left(\mathbf{F}^{-T}\cdot\mathbf{H}\right), \tag{16}$$

where it can be differentiated the addition of the linear term proportional to the magnetic field vector (Maxwell) and a magnetization term described as a hyperbolic tangent profile. The resulting Eulerian magnetization function reads as

$$\mathbf{m}\left(\mathbf{h}\right)=m_s\tanh\left(\frac{\chi}{m_s}\left|\mathbf{h}\right|\right)\frac{\mathbf{h}}{|\mathbf{h}|}, \tag{17}$$

where $|\mathbf{h}|$ represents the magnitude of the Eulerian magnetic field vector $\mathbf{h}$.

Remark. If one sets $\chi=0$ in the previous expressions to recover a non-magnetic material (e.g. the polymer incompressible matrix phase), we obtain

$$\mathbf{B}\left(\mathbf{F},\mathbf{H}\right)=\mu_0\,\mathbf{F}^{-1}\cdot\left(\mathbf{F}^{-T}\cdot\mathbf{H}\right) \tag{18}$$

or simply $\mathbf{b}=\mu_0\mathbf{h}$ by use of (3). In addition, this implies that the magnetization is $\mathbf{m}=\mathbf{0}$ in that case.

3.3.3. Viscous flow rule

To complete the constitutive formulation, we need to define a consistent viscous flow rule to describe the evolution of the internal variable $\mathbf{F}_v$. From the generalized standard materials framework, the constitutive relation dictating the evolution of the internal variable is given by Eq. (12) and the

following coupled equation

$$\frac{\partial \Psi}{\partial \mathbf{F}_v} + \frac{\partial \mathcal{D}}{\partial \dot{\mathbf{F}}_v} = \mathbf{0}. \tag{19}$$

In this work the dissipation potential used is prescribed by

$$\mathcal{D}(\dot{\mathbf{F}}_v, \mathbf{F}_v) = \frac{\tau_v}{\sqrt{2}} \mathbf{D}_v \cdot \mathbf{D}_v, \tag{20}$$

where the viscous rate deformation tensor is imposed following [58]

$$\mathbf{D}_v = \mathbf{F}_e \cdot \dot{\mathbf{F}}_v \cdot \mathbf{F}_v^{-1} \cdot \mathbf{F}_e^{-1} = \frac{1}{\sqrt{2}\tau_v} \text{dev}\left(\boldsymbol{\sigma}^v_{mech}\right) \tag{21}$$

where τ_v is the viscosity of the corresponding phase and $\text{dev}\left(\boldsymbol{\sigma}^v_{mech}\right) = \text{dev}\left(J^{-1}\mathbf{P}^v_{mech} \cdot \mathbf{F}^T\right)$ stands for the deviatoric part of the viscous Cauchy stress. The final expression for the evolution of the viscous deformation gradient reads as

$$\dot{\mathbf{F}}_v = \mathbf{F}_e^{-1} \cdot \mathbf{D}_v \cdot \mathbf{F}_e \cdot \mathbf{F}_v \tag{22}$$

An equivalent formulation that uses the right Cauchy-Green version of $\mathbf{F}_v$, $\mathbf{C}_v = \mathbf{F}_v^T \cdot \mathbf{F}_v$ and thus leads to a smaller number of evolution equations can be found in [59]. Note that the formulation used provides consistent results (incompressible viscous deformation gradients) due to the implicit monolithic framework implemented (see Sections 3.4.3 and 4.1).

3.4. Periodic homogenization problem

This section introduces the homogenization framework for estimating the magneto-mechanical behavior of MREs composed of a soft viscoelastic matrix and magnetic fillers.

3.4.1. Homogenization fundamentals

We consider a magneto-visco-elastic deformable volume occupying a periodic domain Ω_0 in the material (reference) configuration. It contains, in general, different phases, which are distributed randomly or periodically in Ω_0 constituting a representative volume element (RVE). The representativity of the domain is usually a function of the constitutive response of the constituents (e.g.,

linear, nonlinear, coupled or uncoupled) as well as of the average quantity that one is interested in analyzing. For a more detailed discussion on MREs, one is referred to [47].

In all cases, the phases are set at the boundaries of the domain in such a way that Ω_0 may be reproduced periodically in three dimensions, but may be entirely random inside Ω_0. The distribution of the phases is a particularly delicate point that has been very recently shown unambiguously [60] to lead to very sensitive responses depending on local characteristics even in linear elasticity. In the present case, the goal is to study the qualitative features of soft MREs and the relative effect of the matrix viscoelasticity upon the coupled magneto-mechanical response. For that reason, we will use in the next section relatively simplified random and periodic particle distributions, as compared to the actual experiments that may exhibit particle clustering (see for instance recent work exhibiting particle clusters in MREs via an AFM surface analysis [61]).

The problem under study is incremental and dissipative in nature as a result of the polymer viscoelasticity and thus an incremental periodic homogenization framework needs to be considered [62, 63, 64, 65, 57]. In this regard, the average deformation gradient $\overline{\mathbf{F}}$ and magnetic field $\overline{\mathbf{H}}$ at a discrete time $\tau \equiv t + \Delta t$ are expressed in terms of the volume averages of the corresponding local quantities, such that

$$\overline{\mathbf{F}}_\tau = \frac{1}{|\Omega_0|}\int_{\Omega_0} \mathbf{F}_\tau(\mathbf{X})\ \mathrm{d}\Omega_0, \qquad\qquad \overline{\mathbf{H}}_\tau = \frac{1}{|\Omega_0|}\int_{\Omega_0} \mathbf{H}_\tau(\mathbf{X})\ \mathrm{d}\Omega_0, \tag{23}$$

respectively.

The local displacements $\mathbf{u}_\tau(\mathbf{X})$ and magnetic scalar potential $\phi_\tau(\mathbf{X})$ are additively decomposed into linear (macroscopic) and higher order (microscopic fluctuation) contributions

$$\mathbf{u}_\tau(\mathbf{X}) = (\overline{\mathbf{F}}_\tau - \mathbf{I})\cdot\mathbf{X} + \widetilde{\mathbf{u}}_\tau(\mathbf{X}) \qquad \text{and} \qquad \phi_\tau(\mathbf{X}) = -\overline{\mathbf{H}}_\tau\cdot\mathbf{X} + \widetilde{\phi}_\tau(\mathbf{X}), \qquad \forall\ \mathbf{X}\in\Omega_0, \tag{24}$$

where $\widetilde{\mathbf{u}}_\tau(\mathbf{X})$ and $\widetilde{\phi}_\tau(\mathbf{X})$ are the fluctuation fields. Their average over Ω_0 must vanish to obtain (23); a requirement that is automatically fulfilled for Ω_0-*periodic* fluctuation fields.

Each phase is described by known constitutive parameters that determine the behavior at any point $\mathbf{X} \in \Omega_0^{phase}$. The objective of the numerical homogenization is then to resolve the local

displacement and magnetic potential fields in the RVE such that they fulfill the equilibrium and Maxwell equations locally while satisfying certain periodic boundary conditions. The starting point of the homogenization is the definition of the incremental potential

$$\mathcal{W}(\mathbf{F}_\tau, \mathbf{H}_\tau, \mathbf{X}) = \inf_{\mathbf{F}_v^\tau} \int_t^\tau \left\{ \dot{\Psi}\left(\mathbf{F}, \mathbf{H}, \mathbf{F}_v, \mathbf{X}\right) + \mathcal{D}(\dot{\mathbf{F}}_v, \mathbf{F}_v, \mathbf{X}) \right\} \mathrm{d}t, \qquad \mathbf{F}_v(t) = \mathbf{F}_v^t. \tag{25}$$

Here, the dissipation potential $\mathcal{D}$ takes the simple form of Eq. (20), such that $\mathrm{dev}\left(\boldsymbol{\sigma}_{mech}^v\right) = \partial\mathcal{D}/\partial\mathbf{D}_v$, and $\mathbf{D}_v$ are consistent with (21).

Given the optimality of the local incremental potential with respect to the internal variables and the local incompressibility constraint in (10), one may define the admissible sets $\mathcal{K}$ and $\mathcal{G}$ for $\mathbf{u}$ and ϕ, respectively, as

$$\mathcal{K}(\overline{\mathbf{F}}_\tau) = \left\{ \mathbf{u}_\tau = (\overline{\mathbf{F}}_\tau - \mathbf{I}) \cdot \mathbf{X} + \widetilde{\mathbf{u}}_\tau, \det \mathbf{F}_\tau = 1, \ \widetilde{\mathbf{u}}_\tau \text{ periodic in } \Omega_0 \right\} \tag{26}$$

and

$$\mathcal{G}(\overline{\mathbf{H}}_\tau) = \left\{ \phi_\tau = -\overline{\mathbf{H}}_\tau \cdot \mathbf{X} + \widetilde{\phi}_\tau, \ \widetilde{\phi}_\tau \text{ periodic in } \Omega_0 \right\}. \tag{27}$$

We note that the incompressibility constraint $\det \mathbf{F}_\tau = 1$ may be implemented in various manners[3], considering here an admissible set for the pressure p_τ restricted to be a periodic scalar field in the domain Ω_0. The easiest and at the same time rigorous way is to implement it with the use of a Lagrange multiplier (e.g., a pressure term), such that the incremental homogenized potential, $\overline{\mathcal{W}}$, takes the form [66]

$$\overline{\mathcal{W}}(\overline{\mathbf{F}}_\tau, \overline{\mathbf{H}}_\tau) = \inf_{\mathbf{u}_\tau \in \mathcal{K}(\overline{\mathbf{F}}_\tau)} \sup_{\phi_\tau \in \mathcal{G}(\overline{\mathbf{H}}_\tau)} \sup_{p_\tau} \left[\frac{1}{|\Omega_0|} \int_{\Omega_0} \left[\mathcal{W}\left(\mathbf{F}_\tau, \mathbf{H}_\tau, \mathbf{X}\right) - p_\tau (\det \mathbf{F}_\tau - 1) \right] \mathrm{d}\Omega_0 \right]. \tag{28}$$

[3]Unlike the simpler case of pure hyperelasticity, the incompressibility constraint may be implemented in an incremental problem in various ways. For instance, one may impose the constraint at time t or time τ, or even via the time increment $\dot{\mathbf{F}}$.

Applying then the Hill–Mandel lemma in the last expression, we recover readily the macroscopic constitutive relations

$$\overline{\mathbf{P}}_\tau = \frac{\partial \overline{\mathcal{W}}}{\partial \overline{\mathbf{F}}_\tau}(\overline{\mathbf{F}}_\tau, \overline{\mathbf{H}}_\tau) - \overline{p}_\tau \overline{\mathbf{F}}_\tau^{-T}, \qquad \overline{\mathbf{B}}_\tau = -\frac{\partial \overline{\mathcal{W}}}{\partial \overline{\mathbf{H}}_\tau}(\overline{\mathbf{F}}_\tau, \overline{\mathbf{H}}_\tau). \tag{29}$$

In the first equation, $\overline{p}_\tau$ is the average pressure in the RVE. For completeness, we note that the initial conditions of the problem may be set $\overline{\mathbf{F}}_0 = \mathbf{I}$ and $\overline{\mathbf{H}}_0 = \mathbf{0}$.

3.4.2. Macroscopic boundary conditions and potential energy

The loading conditions of the problem are introduced by controlling: i) the average values of the independent macroscopic variables, i.e., applied fields, $(\overline{\mathbf{F}}_\tau^{app}, \overline{\mathbf{H}}_\tau^{app})$; ii) the applied conjugate macroscopic variables, $(\overline{\mathbf{P}}_\tau^{app}, \overline{\mathbf{B}}_\tau^{app})$; iii) a combination of them keeping always one mechanical and one magnetic variable as unknowns. In addition, as we will see in the following, one may also control the Eulerian parts of some of the above quantities, e.g., $\overline{\mathbf{b}}$, $\overline{\mathbf{h}}$ or $\overline{\boldsymbol{\sigma}}$. In any case, it is important that the proposed framework allows for controlling mixed boundary conditions by means of average mechanical stress/strain or magnetic flux/intensity in the current or the reference configurations. In the work of Danas [47] (see also [49, 65]), it has been extensively discussed that in magneto-elastic RVE problems that one is interested in the pure particle-particle interactions, only the mechanical average stress may be controlled, whereas the corresponding Maxwell stresses are automatically equilibrated by imposing continuity of the magnetic fields in neighboring RVEs. Following those studies, we write a potential energy for the RVE that reads

$$\mathcal{P}(\overline{\mathbf{F}}_\tau, \overline{\mathbf{H}}_\tau) = \overline{\mathcal{W}}(\overline{\mathbf{F}}_\tau, \overline{\mathbf{H}}_\tau) - \overline{\mathbf{P}}_\tau^{app} \cdot \left(\overline{\mathbf{F}}_\tau - \mathbf{I}\right) - \overline{\mathbf{H}}_\tau^{app} \cdot \overline{\mathbf{B}}_\tau. \tag{30}$$

Remark. The incremental potential energy (30) is valid when one controls $\overline{\mathbf{P}}$ and $\overline{\mathbf{B}}$, i.e., the last two terms serve as the external "force" loads. If instead, $\overline{\mathbf{F}}$ and $\overline{\mathbf{H}}$ are prescribed, the last two terms are readily omitted. A combination of components from any of the previous average quantities may be prescribed. In that case, the potential energy $\mathcal{P}$ needs to be amended accordingly.

3.4.3. Implementation of the field equations

The governing equations of the global problem are obtained from the optimization of the incremental homogenized potential, $\overline{\mathcal{W}}$ defined in eq. (28). When accounting for periodic boundary conditions, the boundary flux terms vanish due to the effect of opposite periodic boundaries, and, in the absence of body forces, the resulting differential equations are significantly simplified yielding

$$\begin{aligned} \frac{\partial \overline{\mathcal{W}}}{\partial \widetilde{\mathbf{u}}_\tau} &= \nabla_0 \cdot \mathbf{P}\left(\mathbf{F}_\tau, \mathbf{H}_\tau, p_\tau, \mathbf{F}_v^\tau, \mathbf{X}\right) = \mathbf{0} \\ \frac{\partial \overline{\mathcal{W}}}{\partial \widetilde{\phi}_\tau} &= \nabla_0 \cdot \mathbf{B}\left(\mathbf{F}_\tau, \mathbf{H}_\tau, \mathbf{X}\right) = 0 \\ \frac{\partial \overline{\mathcal{W}}}{\partial p_\tau} &= \det \mathbf{F}_\tau - 1 = 0. \end{aligned} \tag{31}$$

Then, for the averaged stress or magnetic density flux control, eq. (30) is considered imposing the macroscopic variables via

$$\begin{aligned} \frac{\partial \mathcal{P}}{\partial \overline{\mathbf{F}}_\tau} &= \frac{1}{|\Omega_0|}\int_{\Omega_0} \mathbf{P}\left(\mathbf{F}_\tau, \mathbf{F}_v^\tau, p_\tau, \mathbf{X}\right)\ \mathrm{d}\Omega_0 - \overline{\mathbf{P}}_\tau^{app} = 0 \\ \frac{\partial \mathcal{P}}{\partial \overline{\mathbf{H}}_\tau} &= \frac{1}{|\Omega_0|}\int_{\Omega_0} \mathbf{B}\left(\mathbf{F}_\tau, \mathbf{H}_\tau, \mathbf{X}\right)\ \mathrm{d}\Omega_0 - \overline{\mathbf{B}}_\tau^{app} = 0. \end{aligned} \tag{32}$$

It is noted here that the total first Piola-Kirchhoff stress is split into a purely mechanical $\overline{\mathbf{P}}_{mech}$ and a Maxwell part $\overline{\mathbf{P}}_{maxw}$, i.e., $\overline{\mathbf{P}} = \overline{\mathbf{P}}_{mech} + \overline{\mathbf{P}}_{maxw}$. The latter is defined in terms of the applied magnetic fields and deformation gradients and is readily obtained from relation (15). For the sake of consistency, $\overline{\mathbf{P}}_\tau^{app}$ refers to the total stress accounting for both mechanical and Maxwell average stresses applied.

Additionally, the evolution of the internal variable must be obtained using the viscous flow rule (Eq. 22). In this work, this evolution is implicitly solved inside the global system of non-linear equations by defining a residual $\mathcal{R}_v$ as [58]

$$\mathcal{R}_v\left(\mathbf{F}_\tau, \mathbf{F}_v^\tau, \mathbf{X}\right) = \mathbf{F}_v^\tau - \mathbf{F}_v^t - \mathbf{F}_e^{\tau\ -1} \cdot \mathbf{D}_v^\tau \cdot \mathbf{F}_e^\tau \cdot \mathbf{F}_v^\tau = 0 \tag{33}$$

where $\dot{\mathbf{F}}_v = \mathbf{F}_v^\tau - \mathbf{F}_v^t$ represents the rate of viscous deformation gradient defined in Eq. (22). For solving the non-linear equilibrium, Eqs. (31), (32) and (33) are expressed in their integral weak form, and the domain Ω_0 is discretized into a FEM mesh to yield into a non-linear discrete system of equations. The non-linear equations are solved using a fully implicit time discretization scheme and the Newton-Raphson procedure to obtain the global equilibrium state at those particular boundary conditions of the corresponding time increment.

4. Numerical results at the microscale and discussion

This section is intended to shed light on the understanding of the behavior of the soft MREs discussed in Section 2. The low stiffness of the matrix used (≈ 1 kPa) hinders the convergence of the problem significantly due to the very large phase contrast. However, this low stiffness improves the potential applications leading to low magnetic thresholds to activate magneto-mechanical couplings ($\approx$ 5 to 100 mT). To this end, the microstructural modeling framework (Section 3) is used for simulating the mechanical and magnetic behavior of soft MREs. First, a mechanical validation is presented, for uniaxial compression tests, followed by compression relaxation tests results. Then the magneto-mechanical interactions are studied from magnetic ramp tests. Finally, the results of cyclic shear tests under magnetic fields are presented. It should be pointed out here that the present experimental setup both in the purely mechanical and magneto-mechanical case, leads to fairly uniform magnetic and mechanical fields in the largest part of the specimen, except very close to the boundaries that barreling and fringe effects may be present (see relevant details of the close-loop magnetic system used in Section 2). Nevertheless, the latter contribute only weakly to the overall force measure. This is a direct consequence of the specimen shape which is rather thin as well as the fact that the magnetic field is directly applied (and controlled in a close-loop fashion) to the boundary of the solid and not far from it (see corresponding discussion on far field simulations and nonuniform magneto-mechanical fields in [54]). These aspects also have a relevant impact on the computation of the Maxwell stress contribution, that may be hypothesized as constant within the MRE sample from a homogenized point of view, see Figure 3. Overall, the experimental setup used herein provides very homogeneous conditions during magneto-mechanical tests, which helps

us obtaining more direct relations between the experiments and the homogenized computational results. This point becomes less ideal under free-expansion tests where the upper magnetic yoke is not used. However, the use of a thin cylindrical sample with a small diameter (cases for 4 mm diameter) allows for keeping the homogenization assumption.

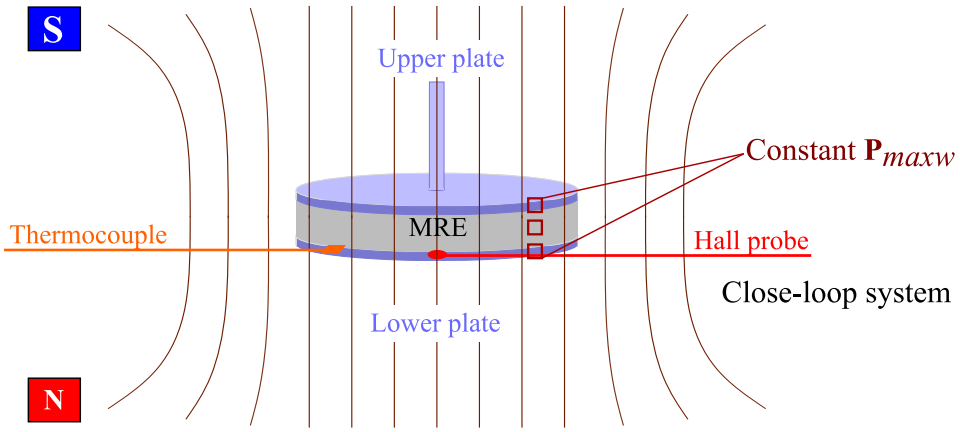

Figure 3: Experimental results for the axially confined tests under axial magnetic fields on cylindrical specimens of 1 mm height and 20 mm diameter. Axial force measured by the load cell of the test machine is plotted versus magnetic induction for three magnetic particle volume fraction $\phi = \{0.1, 0.2, 0.3\}$. The magnetic field is applied at constant rates of 2 and 20 mT/s. Note that the magnetic application rates imposed in these tests provided almost superimposed results without significant differences in their mean curve.

4.1. Numerical FE model

The numerical examples have been carried out using the homogenization framework of Section 3. The material microstructure under study contains two phases, the PDMS matrix and the CIP filler. The constitutive behavior for the matrix is defined as a visco-elastic incompressible solid with null magnetization. In the case of the particles, ideally considered to have a spherical shape, we assume a quasi-rigid solid respond together with a magnetization profile with saturation.

Different idealized particle arrangements have been considered to analyze the microstructural behavior with special alignments of the particles, including random distributions. These include simple cubic (SC), body centered cubic (BCC), face centered cubic (FCC) and random distributions. Figure 4.1 shows the studied cases of particles arrangements for a 20% volume fraction content of CIP. Note that the arrangements are periodic and the study of different volume fractions implies an increase/reduction of the diameter of the particles. In the case of random distributions

of particles, a Monte-Carlo procedure is used for the placement of particles center, avoiding particle overlapping and considering a minimum distance of 10% the radius of the particle.

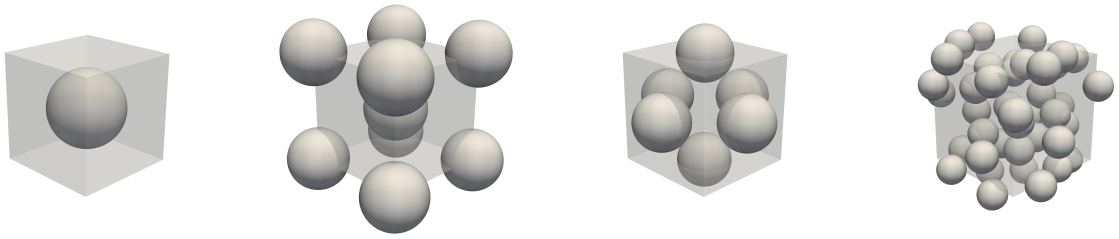

Figure 4: Simple Cubic (SC), Body Centered Cubic (BCC), Face Centered Cubic (FCC), Random (20 particles) distributions containing a 20% v.f. of CIP.

It should be remarked that different random arrangements have been considered, yielding a scatter of 5% in stress-strain curves and lower than 10% in magnetization profiles. The consideration of a higher number of particles would reduce this scatter, but would result in a similar mean curve behavior with a relevant increase in computational cost. For the simulations with random distributions of particles, an RVE with the mean response within the scatter tested has been chosen.

The material parameters selected, all gathered in Table A1, for the behavior of the CIP are $\mu = 81.78\ GPa$ for the shear modulus, $\chi = 30$ for the magnetic susceptibility and $\mu_0 m_s = 2.5\ T$ for the magnetic saturation, which are taken from the literature [67]. As discussed earlier, the particles are considered to be incompressible, a choice that has no effect in the results since the overall mechanical response of the particle is practically rigid as compared to the matrix phase. In turn, the material parameters of the visco-elastic behavior of the matrix have been obtained from the inverse fitting procedure of uniaxial compression curves of PDMS at different rates, resulting in the following values: elastic shear modulus $\mu = 1.03$ kPa, viscous shear modulus $\mu_v = 1.52$ kPa and viscosity $\tau_v = 0.22$ kPa s. All the numerical parameters are summarized in Table 4.1 for the shake of clarity. The domain representing the microstructure is discretized in a FEM mesh of quadratic tetrahedral elements. An adaptive meshing has been used here, where the characteristic length for the elements near the matrix-particle interfaces is set to one eighth of the particle diameter. Note that for the incompressibility condition equation (last term in Eq. 31), the discretization is reduced

to the points corresponding to the tetrahedral elements centers. Additionally, the residual of the viscous flow rule (Eq. 33) is solved at the element integration points.

Phase	Mechanical properties			Magnetic properties	
	Elastic shear modulus μ (kPa)	Viscous shear modulus μ_v (kPa)	Viscosity τ_v (kPa s)	Magnetic susceptibility χ (-)	Magnetic saturation $\mu_0 m_s$ (T)
Matrix	1.03	1.52	0.22	0	—
Particles	81.78×10^6	—	—	30	2.5

Table 1: Mechanical and magnetic properties used for matrix and particle behaviors.

Regarding the numerical implementation, the equilibrium equations (31), (32) and (33) are implemented in the python Finite Elements module FEniCS by symbolically indicating the weak form of those equations and solving the problem monolithically. Moreover, special constraints are imposed in the boundary nodes to accomplish for periodic boundary conditions (Eq. 24). The non-linear problem is then solved with a Newton-Raphson procedure by linearizing in each iteration the non-linear system of equations and solving the resulting linear system by a direct solver. The solution is achieved when either the relative correction in solution or in flux is below the tolerance of $5 \cdot 10^{-3}$. The direct solver is indispensable since the resulting system is ill-posed due to the very large stiffness contrast between the matrix and the particles. Such a novel condition introduced in the present work is a source of instability in the problem, limiting the convergence in simulations under extreme conditions such as high magnetic fields or very large deformations.

To be consistent with common boundary conditions applied in experiments, the Eulerian magnetic field $\overline{\mathbf{b}}$ needs to be imposed. In order to prescribe the macroscopic Eulerian magnetic field $\overline{\mathbf{b}}$ instead of the Lagrangian $\overline{\mathbf{B}}$, one must be cautious. A simple way is to replace the term $\overline{\mathbf{B}}_\tau^{app}$ in Eq. (32) by the analogous expression $\det\left(\overline{\mathbf{F}}_\tau\right) \overline{\mathbf{F}}_\tau^{-1} \cdot \overline{\mathbf{b}}_\tau^{app}$, leading to a fully implicit imposition of $\overline{\mathbf{b}}_\tau^{app}$, which is finally solved during the resolution of the non-linear system. We have validated this procedure to be equivalent to the approaches followed in [47, 49].

As a final remark, the inclusion of the point-wise equation of the viscous residual (eq. 33) into the global system of non-linear equations implies a significant increase of the computational cost. However, in these implementations, the global matrix is saved in sparse format, reducing drastically

the memory requirement, while a sparse solver for the matrix inversion may be readily used. In this regard, the cross-derivative terms are automatically considered for the non-linear solver without a significant computational effort. Moreover, this monolithic approach is able to reach a larger time incrementation compared to other staggered solvers.

4.2. Uniaxial compression

To validate the mechanical behavior resulting from the proposed modeling framework, uniaxial compression tests are performed under different strain rates. The loading path for this test is achieved via mixed stress/strain control, imposing a macroscopic deformation gradient ramp and fixing to zero the macroscopic first Piola-Kirchhoff stress, such that

$$\overline{\mathbf{F}}(t) = \begin{bmatrix} * & * & * \\ 0 & * & * \\ 0 & 0 & 1 + \Delta F_{end} t/t_{end} \end{bmatrix}, \quad \overline{\mathbf{P}}_{mech}(t) = \begin{bmatrix} 0 & 0 & 0 \\ * & 0 & 0 \\ * & * & * \end{bmatrix} \tag{34}$$

where $\Delta F_{end} = 0.2$ is the final stretch increment in the loading direction and the final time t_{end} depends on the strain rate imposed. The different particle arrangements with volume fractions are analyzed. Uniaxial compression tests simulations are compared with experiments at different strain rates in Figures 5 and 6.

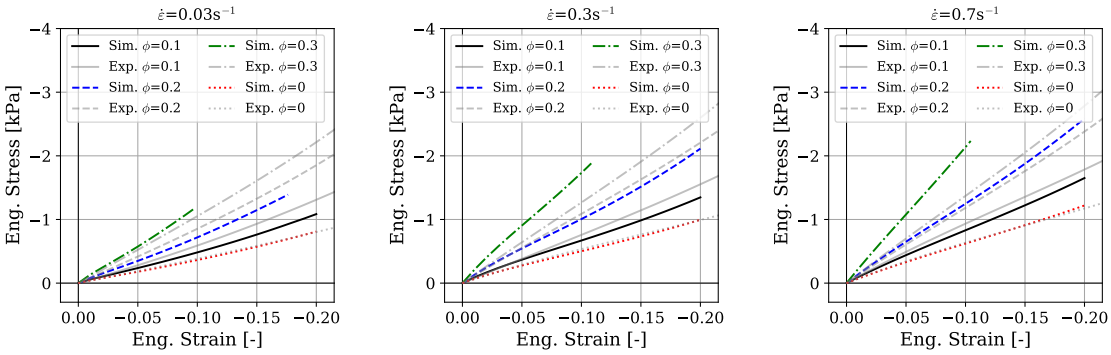

Figure 5: Visco-elastic behavior under uniaxial compression of the PDMS matrix containing different particle v.f. at different rates for SC distributed particles. Comparison between experimental (mean curve of six specimens) and simulation results for different particles volume fractions.

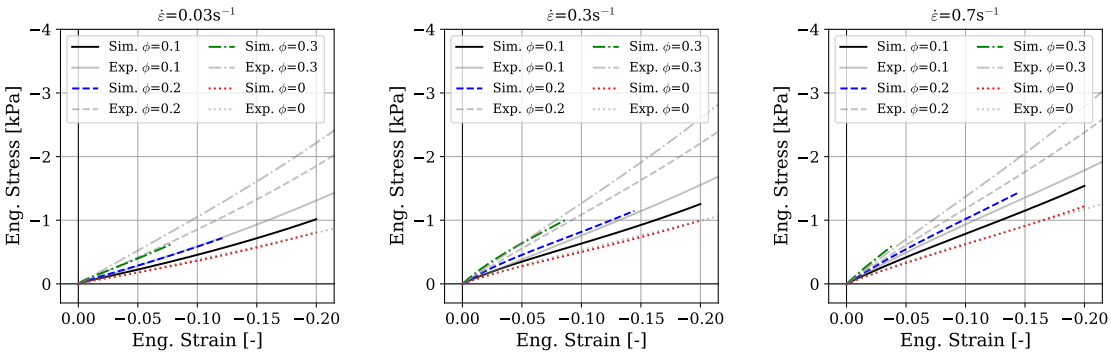

Figure 6: Visco-elastic behavior under uniaxial compression of the PDMS matrix containing different particle v.f. at different rates for randomly distributed 20 particles. Comparison between experimental (mean curve of six specimens) and simulation results for different particles volume fractions.

The random microstructures show the best agreement among the different particle arrangements for the three strain rates studied. For lower particle volume fractions, an underestimation of the stress-strain curve is observed in most of the cases. This fact may be attributed to particle clustering in the actual experimental specimens (see [61]), which are not taken into account in the creation of the numerical microstructures of the present study. Moreover, it can be observed from Figure 5 that the SC arrangements show a stiffer behavior, which is attributed to the special alignment of the particles in the loading direction and reach a compression buckling-type instability. In the case of random distributions, two factors affect the convergence, the small distance between two arbitrary particles that may occur during the generation of the random distributions, and micro-instabilities that may take place within a cluster of particles such as micro locking or local buckling. Moreover, the large stiffness contrast between the matrix and particles ($\approx 10^8$) augments further the possible numerical instabilities. In Figures A.1 and A.2, both the BCC and FCC exhibit a more compliant behavior mainly due to the specific location of the particles, which avoids each other during the application of the loads. It should be noted that phenomenological models [36] may provide more accurate responses but usually including as a trade-off more parameters to fit. In this regard, micromechanical and micromechanical phenomenological models may be considered as complementary, where the former provide insights into the micromechanical interactions and some parameters that calibrated the macroscopic phenomenological model. The latter model is more appropriate for its finally use in technological applications (see a recent work as an example [11]).

4.3. Compression relaxation tests

Using compression relaxation tests, the influence of the particle content on the viscous characteristic relaxation time is analyzed. To this end, macroscopic conditions follow eq. (34) where the deformation gradient (F_{end}) is taken to 0.05 for a $t_{end} = 0.1s$. When the ramp reaches the maximum, a hold time period is applied until the stress is stabilized. Stress-time curves for different particle volume fractions are shown in Figure 7.

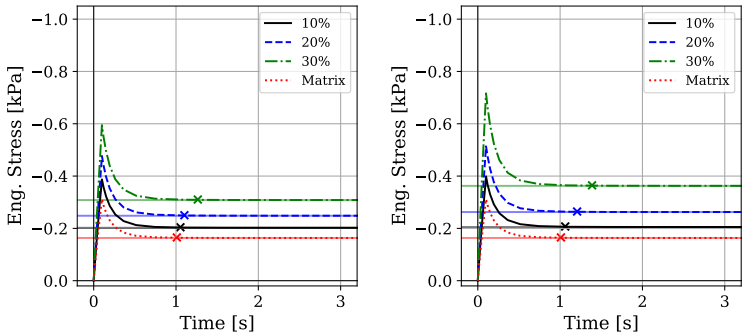

Figure 7: Simulation results of mechanic relaxation behavior of the PDMS matrix containing different particle v.f. for BCC (left) and random (right) distributed particles. The "x" markers indicate the stress stabilization.

It is observed that the characteristic relaxation time increases with the particle content, showing variations of up to 40%. In Figure A.3, the same effect is observed, particularly showing a higher increase of viscous relaxation time in the stiffer particle arrangements (SC). This effect is due to the fact that, for the stiffer particle arrangements, the local concentration of strain is significantly higher, leading to a higher relaxation time within those regions. These tendencies are consistent with the experimental results presented in [27]. Note that different viscous mechanisms may arise from two main sources [68]: 1) different relaxation mechanisms with different characteristic times; 2) as a consequence of heterogeneous distributions of the strain and strain rates within the elastomeric matrix. The latter is nicely captured by our micromechanical modelling framework and show how these models may help us to motivate phenomenological approaches or gain microstructural insights. In this regard, although the same viscosity and, therefore, relaxation time, is considered for the elastomeric phase in all the tested cases, Figure 7 shows how the microstructural arrangement and

volume fraction of the magnetic particles contribute to modulate the macroscopic (homogenized) viscoelastic response of the MRE. These results present higher relaxation times for higher particles' content, demonstrating how microstructural heterogeneity of the strain and strain rate distributions impacts the macroscopic viscoelastic response.

4.4. Magnetostriction tests

Under magnetic fields, the MRE deforms freely due to the magnetic particle interactions and resulting rearrangements. In this case, the effect of the rate of magnetic field application is analyzed. The magnetostriction test consists in a magnetic ramp at different rates with stress-free boundary conditions, followed by a hold time period of magnetic field. The imposition of the magnetic field is performed via Eulerian magnetic flux following

$$\overline{\mathbf{b}}(t) = \begin{Bmatrix} 0 \\ 0 \\ b_{end}t/t_{ramp} \end{Bmatrix}, \quad \overline{\mathbf{P}}_{mech}(t) = \begin{bmatrix} 0 & 0 & 0 \\ * & 0 & 0 \\ * & * & 0 \end{bmatrix}, \quad \overline{\mathbf{F}}(t) = \begin{bmatrix} * & * & * \\ 0 & * & * \\ 0 & 0 & * \end{bmatrix}, \tag{35}$$

where $b_{end} = 15\text{mT}$ and t_{ramp} varies as a function of the magnetic ramp rate, and the relaxation hold time is set to be $t_{hold} = 100 * t_{ramp}$ with a constant b_{end}. The stretch-time curves at different ramp rates are shown in Figure 8. Note that the very soft nature of the matrix used in this work allows for significant magneto-mechanical coupling at small external magnetic fields. This is an important point for further applications as it reduces complexities associated to the generation of such magnetic fields.

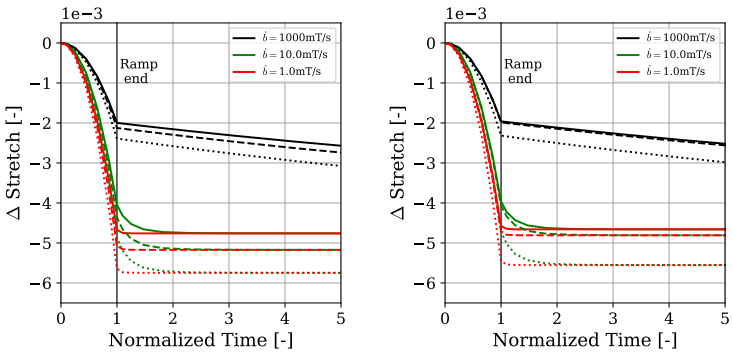

Figure 8: Simulation results of magnetic ramp and hold behavior of the PDMS matrix containing different particle v.f. (solid 10%, dashed 20%, dotted 30%) at different rates for SC (left) and random (right) distributed particles.

The simulations presented in Figures 8 and A.4 show a continuous increase in MRE stretch with the application of the magnetic field, being the deformation a contraction for all the cases. This stretch adopts a maximum stable value for the slowest rate at the moment that the magnetic field reaches its maximum magnitude. When the application rate of the magnetic field is increased, the viscous behavior of the polymeric matrix kicks in resulting in the stiffening of this phase. In such scenarios, the stiffening due to strain rate dependence leads to a temporal constraint in the MRE deformation. As a consequence, the stretch experienced at the end of the magnetic ramp is lower when increasing the application magnetic rate. Thereafter, viscoelastic relaxation mechanisms within the matrix phase contribute to a continuous decrease in stiffness accompanied by a stretching until the full viscous relaxation is achieved. Finally, when the response is stationary, the final deformed configuration is the same for all the rates of magnetic ramp applied, after the proper relaxation time.

It must be remarked that, when imposing an Eulerian magnetic flux, the RVE is subjected to a magnetic field which can be significantly higher for lower particles volume fraction, since the resulting macroscopic magnetic field is inversely proportional to the effective macroscopic magnetic permeability. Thus, in some cases, deformation due to the same magnetic flux can be similar or even larger in the RVE with lower particle content (see FCC in Figure A.4).

4.5. Magnetic relaxation tests

An alternative test allowing to analyze the magneto-visco-elastic interactions is the application of a magnetic ramp while constraining the mechanical deformation. The test consists in a magnetic ramp at different rates with null deformation followed by a hold time of magnetic field, given by

$$\overline{\mathbf{b}}(t) = \begin{Bmatrix} 0 \\ 0 \\ b_{end}t/t_{ramp} \end{Bmatrix}, \quad \overline{\mathbf{F}}(t) = \begin{bmatrix} 1 & 0 & 0 \\ 0 & 1 & 0 \\ 0 & 0 & 1 \end{bmatrix}, \tag{36}$$

where $b_{end} = 15\text{mT}$ and t_{ramp} varies as a function of the magnetic ramp rate with a relaxation hold time of $t_{hold} = 100 * t_{ramp}$ with a constant b_{end}. The stress-time curves at different ramp rates are shown in Figure 9. Note that these simulations are representative, at the microscale, of the experiments shown in Figure 2.

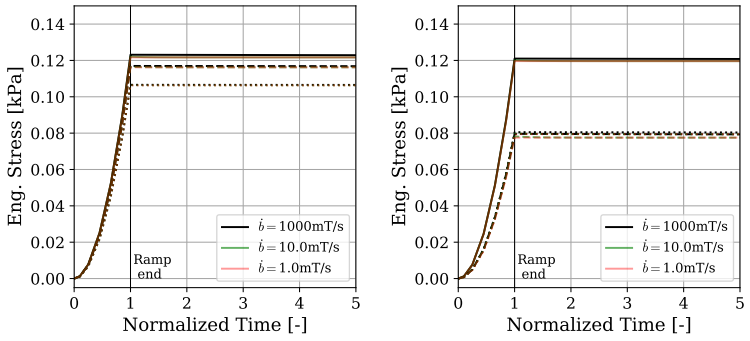

Figure 9: Simulation results of magnetic ramp and hold behavior of the PDMS matrix containing different particle v.f. (solid 10%, dashed 20%, dotted 30%) at different rates for BCC (left) and random (right) distributed particles.

As in the case of the magnetostriction test, Figures 9 and A.5 show that for the stabilized stress (steady state), there is no effect of the rate of the magnetic ramp. However, in contrast to magnetostriction, differences in the stress-time curve during the ramp at different rates are almost negligible, leading to the conclusion that internal stresses are almost time-independent and the internal viscous relaxations are negligible. This is consistent with the experiments presented herein for the magnetic rates tested (Figure 2). Again, it is observed that the RVEs of lower particle content are subjected to significantly higher magnetic fields due to the lower effective magnetic

permeability.

4.6. Cyclic shear tests under magnetic fields

The last tests used to analyze the effect of magnetic fields on the viscous behavior are cyclic shear loops. The RVE is subjected first to a slow magnetic field ramp followed by several cycles of shear. This test is described by imposing the following macroscopic variables

$$\overline{\mathbf{b}}(t) = \begin{Bmatrix} 0 \\ 0 \\ b_{end} \end{Bmatrix}, \quad \overline{\mathbf{F}}(t) = \begin{bmatrix} * & * & 0 \\ 0 & * & F_{max}\sin(\omega t) \\ 0 & 0 & 1 \end{bmatrix}, \quad \overline{\mathbf{P}}_{mech}(t) = \begin{bmatrix} 0 & 0 & * \\ * & 0 & * \\ * & * & * \end{bmatrix}, \tag{37}$$

where F_{max} is the maximum shear deformation achieved during a loop, ω is the angular frequency of the cyclic load and $b_{end} = 50$mT the magnetic field imposed. The shear stress-strain loops in the stabilized regime are shown in Figure 10.

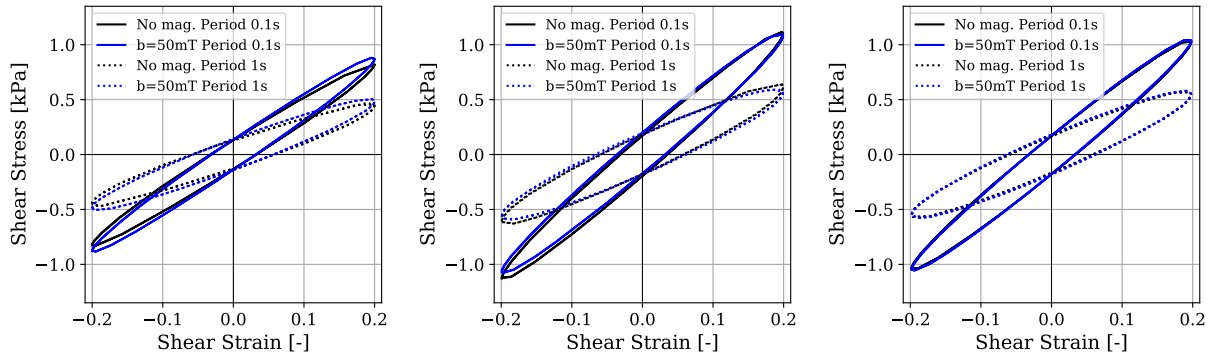

Figure 10: Simulation results of magnetic ramp and shear behavior of the PDMS matrix containing 30% particle v.f. at different rates for SC (left), FCC (middle) and BCC (right) distributed particles. Period 1s: dashed lines; 0.1s: solid lines.

The effect of the magnetic field on the shear loops is small. However, differences can be found in the cases of SC and FCC structures. The SC arrangement presents a stiffening response when applying magnetic fields. This effect is explained by the misalignment of particles that is produced in every shear loop and is not energetically favorable. On the contrary, the FCC provides a softening effect when applying magnetic fields due to the fact that, when shear deformation is applied, the

particles resettle in a more energetically favorable position. Moreover, the effects found in the BCC arrangement are negligible (see Figure 10), leading to almost overlapped shear loops. To perform a fair comparison against a random arrangement of particles a much lower magnetic density flux is imposed (b_{end} = 15mT), as shown in Figures A.6 and A.7. It is observed that for the random arrangement the variation of the viscous cyclic behavior is almost negligible compared to the effect observed in 50mT tests but, in this case, the random arrangement behaves similar to the BCC arrangement, showing a small softening when subjected to a magnetic field.

Finally, the magnetization behavior is analyzed for the studied particle arrangements. In this case, the magnetization module is larger for the higher particle content. Figure 11 shows the Eulerian magnetization (q. 4) variation during the cyclic load normalized by the magnetization at the end of the magnetic ramp. For the SC arrangement, the relative magnetization clearly decreases when the shear strain is maximum. This decrease is due to the misalignment of the particles during shearing. By contrast, the FCC presents an increase of magnetization for the maximum shear, due to the more aligned configuration under shear deformation. From Figure A.8, similar conclusions are obtained for the BCC and random particles arrangements.

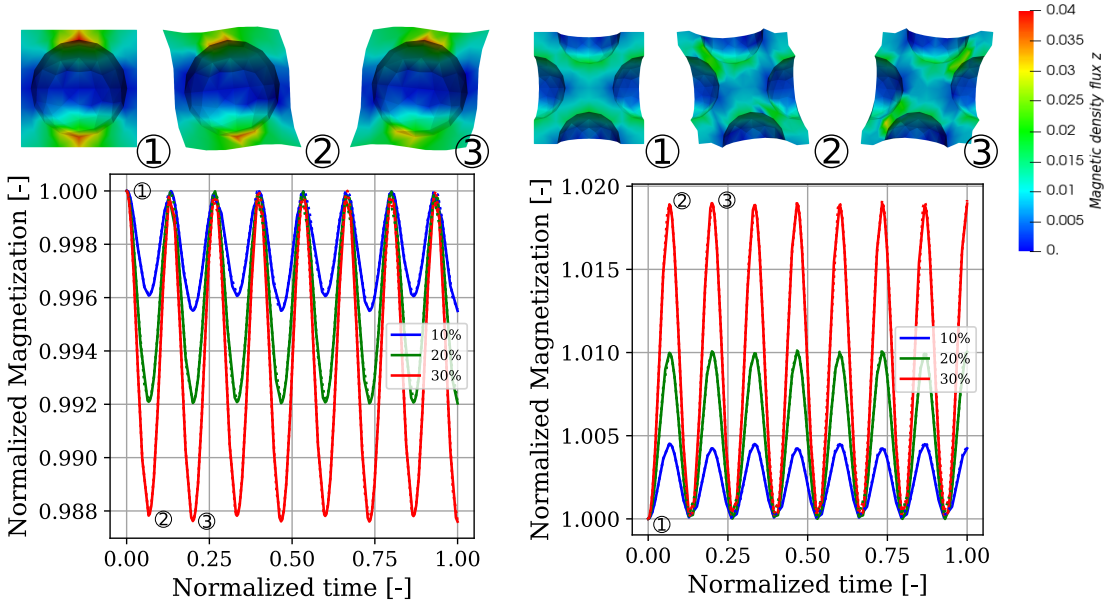

Figure 11: Simulation results of magnetization oscillations during shear deformation of the PDMS matrix containing different particle v.f. at different rates for SC (left) and FCC (right) distributed particles. Period 1s: dashed lines; 0.1s: solid lines. On the upper part, captions of the local magnetic density flux along the direction of the applied magnetic field.

5. Discussion: reconciling microstructural modeling with macrostructural experiments

By comparing Sections 2 and 4, we identify significant discrepancies between the results obtained from the macroscopic experiments and the microstructural modeling. These discrepancies relate to the magnetorheological effect and magnetostrictive nature of the extremely soft MREs tested. The experimental magnetic ramp tests show a clear expansion behavior in the direction of the magnetic field application (see Figure 1). On the contrary, the simulated response of RVEs under magnetic fields shows a compressive magnetostriction effect as depicted in Figure 8. Similar discrepancies are found in the shear tests under magnetic fields. The experimental works show a stiffening behavior [69, 70, 27], while our modeling results indicate that both stiffening/softening responses can be achieved depending on the particle arrangement (Figure 10). In the following, we summarize the relevant works in the literature addressing this problem and, then, we provide new simulations and analogies to reconcile experiments and microstructural modeling.

In the literature, it has been reported that, under the application of an external magnetic field,

MREs undergo either compressive or tensile strain. Early works discuss that MREs shorten along the magnetic field direction as the particles tend to approximate each other [71, 33, 9]. However, a deeper insight unveils that the magnetostrictive behavior of MREs depends on a wider variety of factors, such as the volume fraction and micro-structural arrangement of the magnetic particles, or the magnetic boundary conditions and the nature of the magnetic field applied [54]. Regarding the influence of the particles distribution, it is reported that contraction of the structure potentially occurs when particles are anisotropically aligned, and expansion when they are isotropically arranged [72, 33, 73]. Besides, magnetostriction has experimentally been observed to be larger for isotropic arrangements than for anisotropic specimens [15]. Moreover, it is accepted that larger particle concentration benefits from greater effective macroscopic elongation [72, 74, 73]. We would like to highlight the work by Guan et al. [7], where cylindrical MRE samples were characterized, observing elongation for any magnetic induction applied. The given explanation suggested that ellipse-shaped magnetic particles rotate to align their magnetic dipoles with the applied field, thus interacting with the carrier matrix and giving macroscopic effective elongation. Han et al. [26] developed a simplified phenomenological model that predicts the experimentally observed elongation of MRE samples, depicting relative magnetic permeability as a function of the axial strain. Another relevant work is due to Liao et al. [75], which focused on determining the axial force that appears when a MRE sample is confined, thus prevented from elongating under the application of external magnetic fields. The importance of the microstructural arrangement of the magnetic particles has been approached by computational models. Several authors studied the sign of the magnetostrictive deformation from a computational microstructural basis [15, 76, 77, 25, 41]. Overall, all these works show the importance of the microstructural arrangement of the magnetic particles on the MRE behavior. However, although these models can explain contraction/expansion transitions, their results often differ from macroscopic observations of the magneto-mechanical response of MREs.

Despite the relevant microstructural features presented above, we suggest the magnetic boundary conditions and nature of the applied field as the crucial factor determining the macroscopic response of the soft MRE. In the literature, some experimental works have approached this matter creat-

ing the magnetic field by means of a permanent magnet (i.e., NdFeB permanent magnet) [78, 9]. In this case, the permanent magnet acts as a magnetic pole and, despite the magnetic particles being attracted to each other as they get magnetized, a parallel effect arises as all the particles feel attracted by the magnetic pole, hence the MRE sample macroscopically compresses. Kalina et al. [74] suggested a size of the free space that surrounds the MRE sample fifteen times larger than the specimen size to guarantee that the magnetization poles and the boundary domain can be neglected [79, 74].

To reconcile microstructure-based models with macroscopic observations, some ad-hoc simulations and experiments have been performed. From microstructural simulations, the attraction between particles is observed for low magnetic fields so that they align forming chain-like structures [47, 80]. Figure 12 shows that, for a BCC arrangement with the middle particle located with a small offset to the center, attraction forces impulse the middle particle to the neighbouring ones, resulting in chain-like spatial distributions. When these particles form such a chain-like structure, this tends to align with the magnetic field driven by a paramagnetic torque. This phenomenon, which becomes stronger for extremely soft matrices, has been investigated in previous works [81, 82, 83]. Making use of the microstructural modeling framework developed herein, we simulate a three-particle chain subjected to a vertical magnetic field. The result of this simulation is presented in Figure 12, where a chain alignment towards the magnetic field direction is observed. As a proof of concept, we take the macroscopic sample from previous experimental work [27], which consists of petals formed by a succession of macroscopic spherical elements. This design aims at emulating the particle chains originated in the microstucture, thus scaling up these geometrical features to the macroscale. When applying the external magnetic field perpendicular to the petals, these experience important macroscopic magnetic torques leading to rotations that push the structure to align along the magnetic field lines (Figure 12). This phenomenon can be translated to the microstructural response in the form of micro-paramagnetic torques affecting different local points. Thus, the sum of these contributions results in an apparent expansion of the samples along the magnetic field direction (Figure 1). In addition, this phenomenon may explain the discrepancies observed by means of magnetorheological effect. When the particles come together forming a chain and this aligns along

the field direction, the resulting microstructural arrangement approaches to the simple cubic (SC) distribution studied. Therefore, under shear loading, less energetically favorable states are reached leading to an apparent stiffening of the MRE (see numerical results in Figure 10 and equivalent experiments presented in previous works [27, 69]).

All in all, the response of extremely soft MREs must be understood as the strong combination of both microstructural and macrostructural responses. For instance, in Lefevre et al. JMPS, 2019, the macroscopic response is affected both by microstructural characteristics (e.g., soft or hard mechanical particles) as well as by the specimen shapes. Although this statement may look general, as this is the case of most materials and especially multifunctional composites, this point is of especial relevance for the studied MREs. The extremely soft nature of the polymeric matrix facilitates the rearrangement of the particles within the MRE. Thus, the material responds locally to external magnetic fields experiencing such microstructural rearrangements that differ within the macroscopic geometry of the sample (as the magnetic field can certainly vary from local-to-local regions of the sample). Therefore, the overall macroscopic response of the MRE needs to be understood as a competition of these microscopic structural formations and how these interact between different local regions of the sample. On top of this complex behavior, viscoelastic effects play a crucial role determining the apparent stiffness of the polymeric phase potentially leading to different equilibrium states.

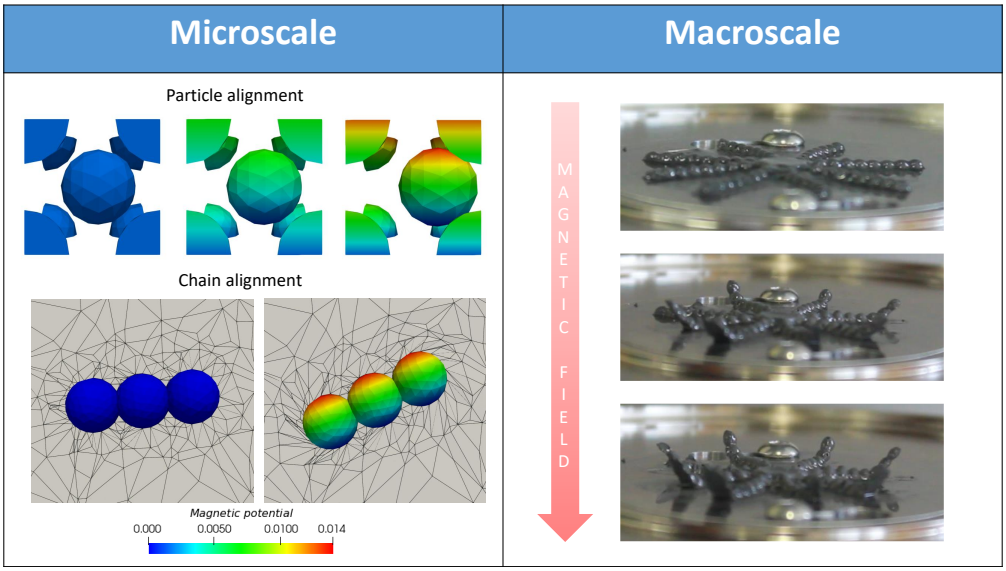

Figure 12: Illustration of the magnetorehological effects at different scales. Microscale: particle alignment under vertical magnetic field and constrained deformation; chain alignment under magnetic fields, from 5 to 30 degrees of inclination. Macroscale: test sample geometry effect. Note that the result for the macroscale deformation has been extracted from [27].

6. Conclusions

The microstructure-based homogenization framework is a powerful tool for the understanding of the behavior of soft MREs. The complex viscous and magnetic responses are shown in the experimental summary presented in Section 2. Under magnetic fields, the MRE shows an expansive behavior parallel to the magnetic field applied. This behavior is due to several contributions: microscopic magnetic particles interactions, formation of mesoscopic structures such as particle chains and the boundary effect due to experimental conditions. From a microscopic mechanical modeling point of view, several conclusions can be drawn: i) the random particle distribution presents the best agreement with experiments; ii) the particle content directly affects the characteristic viscous relaxation time, obtaining higher times for higher particle volume fractions. Under magnetic fields, the microstructural modeling response suggests negligible effects of the rate dependences in the long term (steady) state, although it influences significantly the transient response. Recent experimental work [27] showed that higher magnetic application rates can lead to different equilibrium states due to microstructural blocking phenomena. In this regard, further modeling efforts are needed to overcome convergence issues and allow for extreme microstructural rearrangements. Regarding the

complex shear cyclic tests under magnetic fields, small effect of the magnetic fields is found. For the case of SC, where the particles configuration is clearly aligned with the magnetic field, a stiffening of the shear loop is observed due to the shear misalignment. For the FCC, a contrary effect is observed, due to the more aligned particle position when sheared. After the analysis of microscopic modeling, some outcomes can be taken for the macroscopic behavior. We suggest that, for extremely soft polymeric matrices ($\approx$ 1 kPa), the particles tend to form chains-like distributions and such microstructures then rotate to align with the external magnetic field applied. These phenomena may explain, under magnetic fields: i) the expansive behavior of the soft MREs; and ii) the increase in shear stiffness, reconciling modeling results with experimental observations.

Code

The code developed in this work will be fully available in the final published version with a direct link present in the manuscript.

Acknowledgement

SL, MAMM and DGG acknowledge support from the European Research Council (ERC) under the European Union's Horizon 2020 research and innovation programme (grant agreement No. 947723, project: 4D-BIOMAP). KD acknowledge support from the European Research Council (ERC) under the European Union's Horizon 2020 research and innovation program (grant agreement No. 636903 - MAGNETO). DGG acknowledges support from the Talent Attraction grant (CM 2018 - 2018-T2/IND-9992) from the Comunidad de Madrid and MAMM acknowledges support from the Ministerio de Ciencia, Innovacion y Universidades, Spain (FPU19/03874).

Appendix A. Supplemental Results

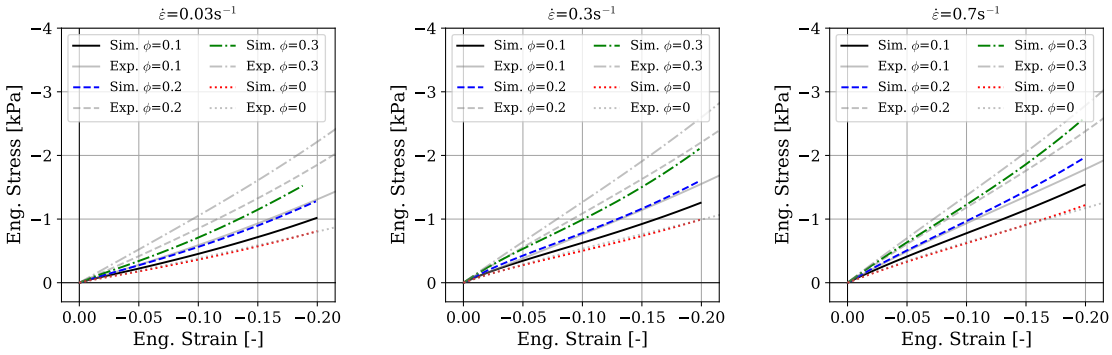

Figure A.1: Visco-elastic behavior under uniaxial compression of the PDMS matrix containing different particle v.f. at different rates for BCC distributed particles. Comparison between experimental (mean curve of six specimens) and simulation results for different particles volume fractions.

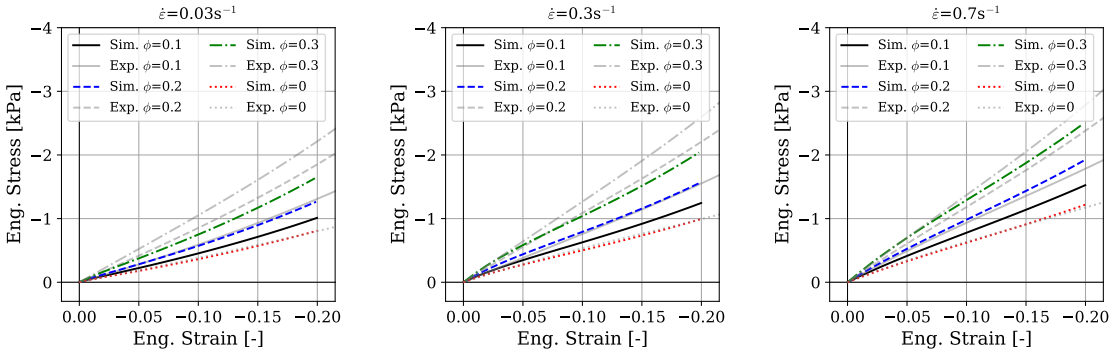

Figure A.2: Visco-elastic behavior under uniaxial compression of the PDMS matrix containing different particle v.f. at different rates for FCC distributed particles. Comparison between experimental (mean curve of six specimens) and simulation results for different particles volume fractions.

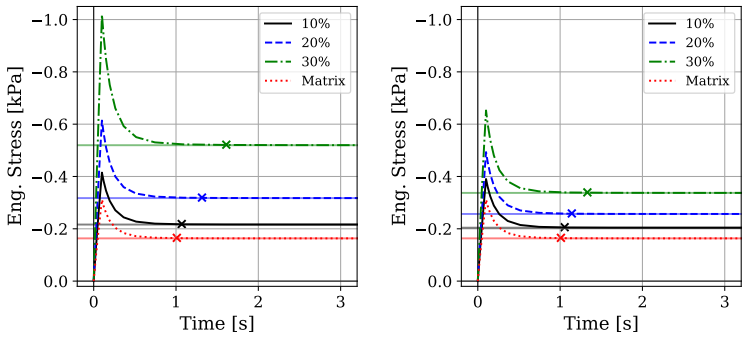

Figure A.3: Simulation results of the mechanic relaxation behavior of the PDMS matrix containing different particle v.f. for SC (left) and FCC (right) distributed particles. The "x" markers indicate the stress stabilization.

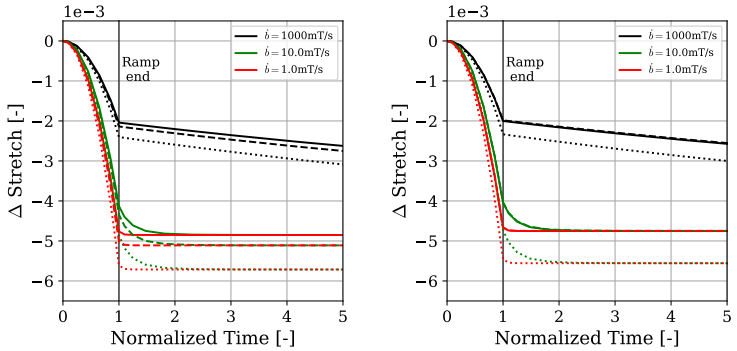

Figure A.4: Simulation results of magnetic ramp and hold behavior of the PDMS matrix containing different particle v.f. (solid 10%, dashed 20%, dotted 30%) at different rates for BCC (left) and FCC (right) distributed particles.

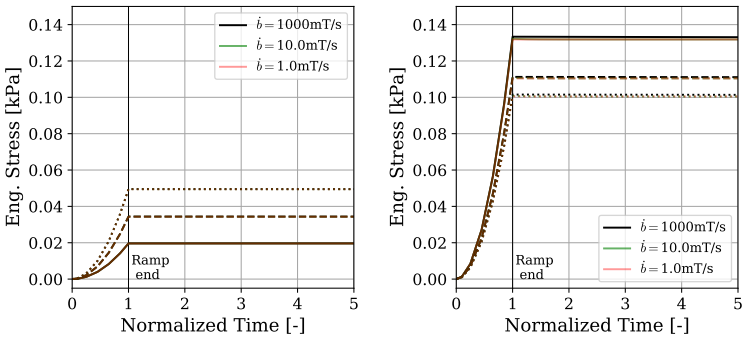

Figure A.5: Simulation results of magnetic ramp and hold behavior of the PDMS matrix containing different particle v.f. (solid 10%, dashed 20%, dotted 30%) at different rates for SC (left) and FCC (right) distributed particles.

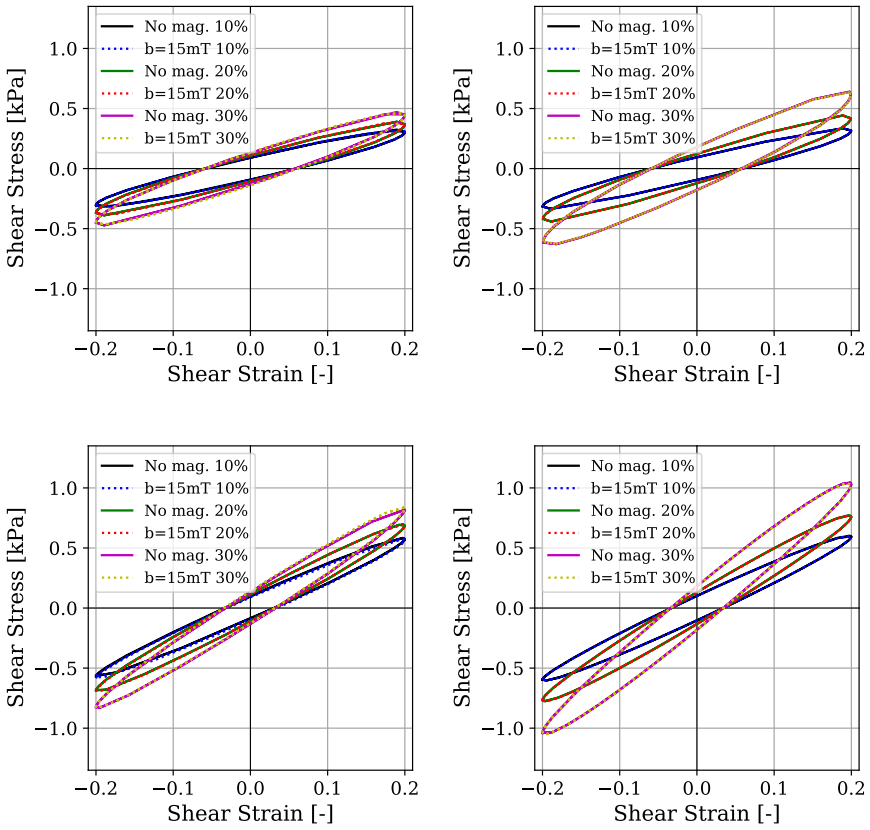

Figure A.6: Simulation results of magnetic ramp and shear behavior of the PDMS matrix containing different particle v.f. at different rates for SC (left) and FCC (right) distributed particles. Periods 1s (top) and 0.1s (bottom).

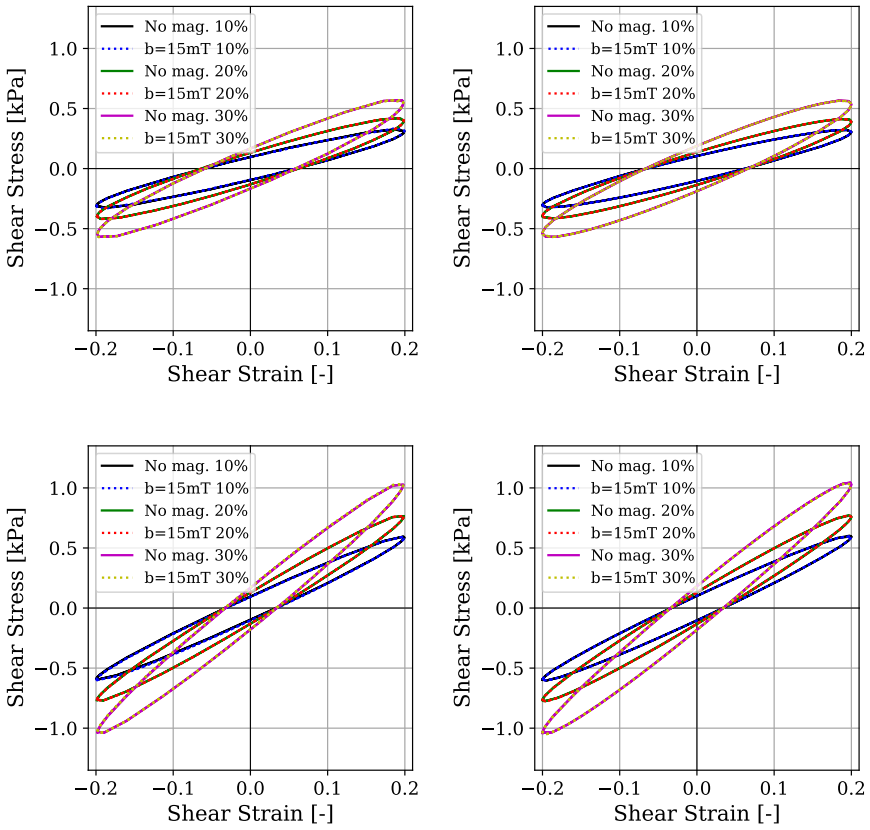

Figure A.7: Simulation results of magnetic ramp and shear behavior of the PDMS matrix containing different particle v.f. at different rates for BCC (left) and random (right) distributed particles. Periods 1s (top) and 0.1s (bottom).

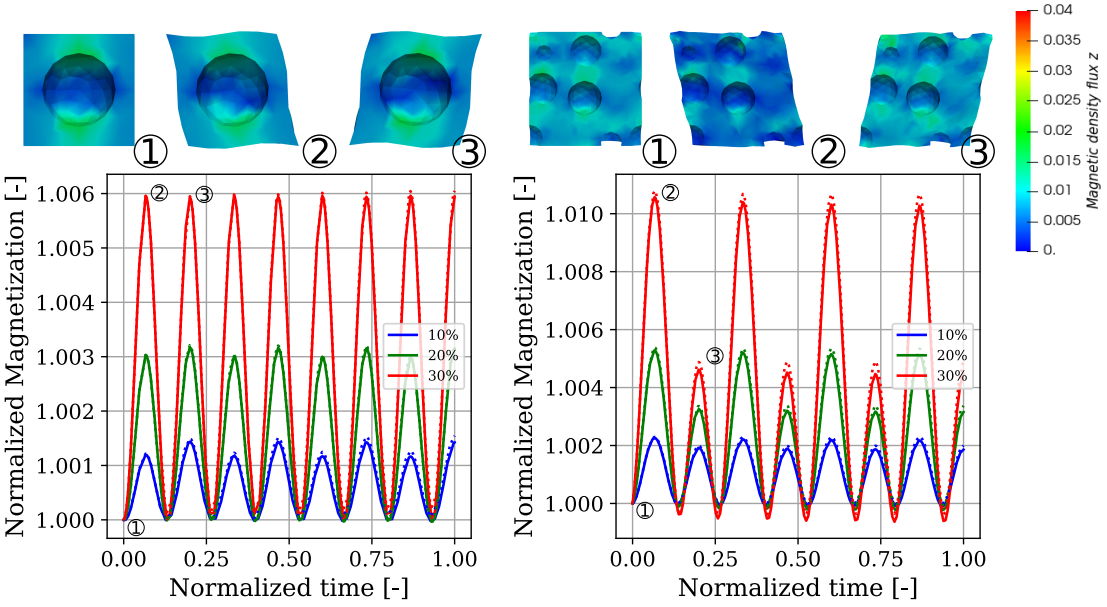

Figure A.8: Simulation results of magnetization oscillations during shear deformation of the PDMS matrix containing different particle v.f. at different rates for BCC (left) and random (right) distributed particles. Period 1s: dashed lines; 0.1s: solid lines. On the upper part, captions of the local magnetic density flux along the direction of the applied magnetic field.

References

[1] W.I. Kordonsky. Magnetorheological effect as a base of new devices and technologies. *Journal of Magnetism and Magnetic Materials*, 122(1):395–398, 1993.

[2] Mark R Jolly, J David Carlson, and Beth C Muñoz. A model of the behaviour of magnetorheological materials. *Smart Materials and Structures*, 5(5):607–614, oct 1996.

[3] Jean-Paul Pelteret and Paul Steinmann. *Magneto-Active Polymers*. De Gruyter, 2019.

[4] S. Abramchuk, E. Kramarenko, G. Stepanov, L. V. Nikitin, G. Filipcsei, A. R. Khokhlov, and M. Zrínyi. Novel highly elastic magnetic materials for dampers and seals: Part i. preparation and characterization of the elastic materials. *Polymers for Advanced Technologies*, 18(11):883–890, 2007.

[5] A. M. Biller, O. V. Stolbov, and Yu. L. Raikher. Mesoscopic magnetomechanical hysteresis in a magnetorheological elastomer. *Phys. Rev. E*, 92:023202, Aug 2015.

[6] Yancheng Li, Jianchun Li, Weihua Li, and Haiping Du. A state-of-the-art review on magnetorheological elastomer devices. *Smart Materials and Structures*, 23(12):123001, nov 2014.

[7] Xinchun Guan, Xufeng Dong, and Jinping Ou. Magnetostrictive effect of magnetorheological elastomer. *Journal of Magnetism and Magnetic Materials*, 320(3):158–163, 2008.

[8] Nicholas Bira, Pallavi Dhagat, and Joseph R. Davidson. A review of magnetic elastomers and their role in soft robotics. *Frontiers in Robotics and AI*, 7:146, 2020.

[9] Xuanhe Zhao, Jaeyun Kim, Christine A. Cezar, Nathaniel Huebsch, Kangwon Lee, Kamal Bouhadir, and David J. Mooney. Active scaffolds for on-demand drug and cell delivery. *Proceedings of the National Academy of Sciences*, 108(1):67–72, 2011.

[10] Zsolt Varga, Genovéva Filipcsei, and Miklós Zrínyi. Magnetic field sensitive functional elastomers with tuneable elastic modulus. *Polymer*, 47(1):227–233, 2006.

[11] Miguel Angel Moreno-Mateos, Jorge Gonzalez-Rico, Emanuel Nunez-Sardinha, Clara Gomez-Cruz, Maria Luisa Lopez-Donaire, Sergio Lucarini, Angel Arias, Arrate Muñoz-Barrutia, Diego Velasco, and Daniel Garcia-Gonzalez. Magneto-mechanical system to reproduce and quantify complex strain patterns in biological materials. *Applied Materials Today*, 27:101437, 2022.

[12] Andrea Stoll, Matthias Mayer, Gareth J. Monkman, and Mikhail Shamonin. Evaluation of highly compliant magneto-active elastomers with colossal magnetorheological response. *Journal of Applied Polymer Science*, 131(2), 2014.

[13] Junru Yao, Youyi Sun, Yan Wang, Qiang Fu, Zhiyuan Xiong, and Yaqing Liu. Magnet-induced aligning magnetorheological elastomer based on ultra-soft matrix. *Composites Science and Technology*, 162:170–179, 2018.

[14] G V Stepanov, D Yu Borin, Yu L Raikher, P V Melenev, and N S Perov. Motion of ferroparticles inside the polymeric matrix in magnetoactive elastomers. *Journal of Physics: Condensed Matter*, 20(20):204121, may 2008.

[15] K. Danas, S.V. Kankanala, and N. Triantafyllidis. Experiments and modeling of iron-particle-filled magnetorheological elastomers. *Journal of the Mechanics and Physics of Solids*, 60(1):120–138, 2012.

[16] Viktor M. Kalita, Andrei A. Snarskii, Mikhail Shamonin, and Denis Zorinets. Effect of single-particle magnetostriction on the shear modulus of compliant magnetoactive elastomers. *Phys. Rev. E*, 95:032503, Mar 2017.

[17] D Günther, D Yu Borin, S Günther, and S Odenbach. X-ray micro-tomographic characterization of field-structured magnetorheological elastomers. *Smart Materials and Structures*, 21(1):015005, dec 2011.

[18] Anil K. Bastola and Mokarram Hossain. A review on magneto-mechanical characterizations of magnetorheological elastomers. *Composites Part B: Engineering*, 200:108348, 2020.

[19] G Y Zhou and Z Y Jiang. Deformation in magnetorheological elastomer and elastomer–ferromagnet composite driven by a magnetic field. *Smart Materials and Structures*, 13(2):309–316, feb 2004.

[20] A. V. Chertovich, G. V. Stepanov, E. Yu. Kramarenko, and A. R. Khokhlov. New composite elastomers with giant magnetic response. *Macromolecular Materials and Engineering*, 295(4):336–341, 2010.

[21] W. H. Li, Y. Zhou, and T. F. Tian. Viscoelastic properties of mr elastomers under harmonic loading. *Rheologica Acta*, 49(7):733–740, Jul 2010.

[22] G.V. Stepanov, S.S. Abramchuk, D.A. Grishin, L.V. Nikitin, E.Yu. Kramarenko, and A.R. Khokhlov. Effect of a homogeneous magnetic field on the viscoelastic behavior of magnetic elastomers. *Polymer*, 48(2):488–495, 2007.

[23] Vladislav V. Sorokin, Gennady V. Stepanov, Mikhail Shamonin, Gareth J. Monkman, Alexei R. Khokhlov, and Elena Yu. Kramarenko. Hysteresis of the viscoelastic properties and the normal force in magnetically and mechanically soft magnetoactive elastomers: Effects of filler composition, strain amplitude and magnetic field. *Polymer*, 76:191–202, 2015.

[24] Siddaiah Yarra, Faramarz Gordaninejad, Majid Behrooz, and Gokhan Pekcan. Performance of natural rubber and silicone-based magnetorheological elastomers under large-strain combined axial and shear loading. *Journal of Intelligent Material Systems and Structures*, 30(2):228–242, 2019.

[25] Lukas Fischer and Andreas M. Menzel. Magnetostriction in magnetic gels and elastomers as a function of the internal structure and particle distribution. *The Journal of Chemical Physics*, 151(11):114906, 2019.

[26] Yi Han, Akshi Mohla, Xiao Huang, Wei Hong, and Leann E. Faidley. Magnetostriction and field stiffening of magneto-active elastomers. *International Journal of Applied Mechanics*, 07(01):1550001, 2015.

[27] M.A. Moreno, J. Gonzalez-Rico, M.L. Lopez-Donaire, A. Arias, and D. Garcia-Gonzalez. New experimental insights into magneto-mechanical rate dependences of magnetorheological elastomers. *Composites Part B: Engineering*, page 109148, 2021.

[28] A.K. Bastola, E. Ang, M. Paudel, and L. Li. Soft hybrid magnetorheological elastomer: Gap bridging between mr fluid and mr elastomer. *Colloids and Surfaces A: Physicochemical and Engineering Aspects*, 583:123975, 2019.

[29] Landau LD. and Lifshitz EM. *Electrodynamics of continuous media.* Oxford, UK: Pergamon Press., 1960.

[30] Livens GH. *The theory of electricity.* 2nd edn. Cambridge, UK: Cambridge University Press., 1962.

[31] Liliana Borcea and Oscar Bruno. On the magneto-elastic properties of elastomer–ferromagnet composites. *Journal of the Mechanics and Physics of Solids*, 49(12):2877–2919, 2001.

[32] A. Dorfmann and R. W. Ogden. Nonlinear magnetoelastic deformations of elastomers. *Acta Mechanica*, 167(1):13–28, Jan 2004.

[33] S.V. Kankanala and N. Triantafyllidis. On finitely strained magnetorheological elastomers. *Journal of the Mechanics and Physics of Solids*, 52(12):2869–2908, 2004.

[34] David J. Steigmann. Equilibrium theory for magnetic elastomers and magnetoelastic membranes. *International Journal of Non-Linear Mechanics*, 39(7):1193–1216, 2004.

[35] Roger Bustamante. Transversely isotropic nonlinear magneto-active elastomers. *Acta Mechanica*, 210(3):183–214, Mar 2010.

[36] Prashant Saxena, Mokarram Hossain, and Paul Steinmann. A theory of finite deformation magneto-viscoelasticity. *International Journal of Solids and Structures*, 50(24):3886–3897, 2013.

[37] Peet Cremer, Hartmut Löwen, and Andreas M. Menzel. Tailoring superelasticity of soft magnetic materials. *Applied Physics Letters*, 107(17):171903, 2015.

[38] Dirk Romeis, Vladimir Toshchevikov, and Marina Saphiannikova. Elongated micro-structures in magneto-sensitive elastomers: a dipolar mean field model. *Soft Matter*, 12:9364–9376, 2016.

[39] Dirk Romeis, Philipp Metsch, Markus Kästner, and Marina Saphiannikova. Theoretical models for magneto-sensitive elastomers: A comparison between continuum and dipole approaches. *Phys. Rev. E*, 95:042501, Apr 2017.

[40] Zhiqiang Xu, Heng Wu, Qiuliang Wang, Liyin Yi, and Jun Wang. Simulation study on the motion of magnetic particles in silicone rubber-based magnetorheological elastomers. *Mathematical Problems in Engineering*, 2019:8182651, Jul 2019.

[41] Daniel Garcia-Gonzalez and Mokarram Hossain. A microstructural-based approach to model magneto-viscoelastic materials at finite strains. *International Journal of Solids and Structures*, 208-209:119–132, 2021.

[42] Daniel Garcia-Gonzalez and Mokarram Hossain. Microstructural modelling of hard-magnetic soft materials: Dipole–dipole interactions versus zeeman effect. *Extreme Mechanics Letters*, 48:101382, 2021.

[43] A. Javili, G. Chatzigeorgiou, and P. Steinmann. Computational homogenization in magneto-mechanics. *International Journal of Solids and Structures*, 50(25):4197–4216, 2013.

[44] C. Spieler, M. Kästner, J. Goldmann, J. Brummund, and V. Ulbricht. Xfem modeling and homogenization of magnetoactive composites. *Acta Mechanica*, 224(11):2453–2469, Nov 2013.

[45] Karl A. Kalina, Philipp Metsch, and Markus Kästner. Microscale modeling and simulation of magnetorheological elastomers at finite strains: A study on the influence of mechanical preloads. *International Journal of Solids and Structures*, 102-103:286–296, 2016.

[46] Marc-Andre Keip and Matthias Rambausek. A multiscale approach to the computational characterization of magnetorheological elastomers. *International Journal for Numerical Methods in Engineering*, 107(4):338–360, 2016.

[47] K. Danas. Effective response of classical, auxetic and chiral magnetoelastic materials by use of a new variational principle. *Journal of the Mechanics and Physics of Solids*, 105:25–53, 2017.

[48] M.-A. Keip and A. Sridhar. A variationally consistent phase-field approach for micro-magnetic domain evolution at finite deformations. *Journal of the Mechanics and Physics of Solids*, 125:805–824, 2019.

[49] Dipayan Mukherjee, Laurence Bodelot, and Kostas Danas. Microstructurally-guided explicit continuum models for isotropic magnetorheological elastomers with iron particles. *International Journal of Non-Linear Mechanics*, 120:103380, 2020.

[50] Marc Leonard, Naibin Wang, Oscar Lopez-Pamies, and Toshio Nakamura. The nonlinear elastic response of filled elastomers: Experiments vs. theory for the basic case of particulate fillers of micrometer size. *Journal of the Mechanics and Physics of Solids*, 135:103781, 2020.

[51] P. Ponte Castañeda and E. Galipeau. Homogenization-based constitutive models for magnetorheological elastomers at finite strain. *Journal of the Mechanics and Physics of Solids*, 59(2):194–215, 2011.

[52] Evan Galipeau and Pedro Ponte Castañeda. A finite-strain constitutive model for magnetorheological elastomers: Magnetic torques and fiber rotations. *Journal of the Mechanics and Physics of Solids*, 61(4):1065–1090, 2013.

[53] Evan Galipeau and Pedro Ponte Castañeda. The effect of particle shape and distribution on the macroscopic behavior of magnetoelastic composites. *International Journal of Solids and Structures*, 49(1):1–17, 2012.

[54] Victor Lefèvre, Kostas Danas, and Oscar Lopez-Pamies. A general result for the magnetoelastic response of isotropic suspensions of iron and ferrofluid particles in rubber, with applications to spherical and cylindrical specimens. *Journal of the Mechanics and Physics of Solids*, 107:343–364, oct 2017.

[55] Victor Lefèvre, Kostas Danas, and Oscar Lopez-Pamies. Two families of explicit models constructed from a homogenization solution for the magnetoelastic response of MREs containing iron and ferrofluid particles. *International Journal of Non-Linear Mechanics*, 119:103362, March 2020.

[56] C. Dorn, L. Bodelot, and K. Danas. Experiments and numerical implementation of a boundary value problem involving a magnetorheological elastomer layer subjected to a nonuniform magnetic field. *Journal of Applied Mechanics*, 88(7), apr 2021.

[57] Kamalendu Ghosh, Bhavesh Shrimali, Aditya Kumar, and Oscar Lopez-Pamies. The nonlinear viscoelastic response of suspensions of rigid inclusions in rubber: I—gaussian rubber with constant viscosity. *Journal of the Mechanics and Physics of Solids*, 154:104544, 2021.

[58] Daniel Garcia-Gonzalez and Chad M. Landis. Magneto-diffusion-viscohyperelasticity for magneto-active hydrogels: Rate dependences across time scales. *Journal of the Mechanics and Physics of Solids*, 139:103934, 2020.

[59] Aditya Kumar and Oscar Lopez-Pamies. On the two-potential constitutive modeling of rubber viscoelastic materials. *Comptes Rendus Mécanique*, 344(2):102–112, February 2016.

[60] O. Zerhouni, S. Brisard, and K. Danas. Quantifying the effect of two-point correlations on the effective elasticity of specific classes of random porous materials with and without connectivity. *International Journal of Engineering Science*, 166:103520, 2021.

[61] X Chang, S Hallais, S Roux, and K Danas. Model reduction techniques for quantitative nano-mechanical AFM mode. *Measurement Science and Technology*, 32(7):075406, may 2021.

[62] M. Ortiz and L. Stainier. The variational formulation of viscoplastic constitutive updates. *Computer Methods in Applied Mechanics and Engineering*, 171(3):419–444, 1999.

[63] Christian Miehe. Strain-driven homogenization of inelastic microstructures and composites based on an incremental variational formulation. *International Journal for Numerical Methods in Engineering*, 55(11):1285–1322, 2002.

[64] Klaus Hackl and Franz Dieter Fischer. On the relation between the principle of maximum dissipation and inelastic evolution given by dissipation potentials. *Proceedings of the Royal Society A: Mathematical, Physical and Engineering Sciences*, 464(2089):117–132, 2008.

[65] Dipayan Mukherjee, Matthias Rambausek, and Kostas Danas. An explicit dissipative model for isotropic hard magnetorheological elastomers. *Journal of the Mechanics and Physics of Solids*, 151:104361, 2021.

[66] Christian Miehe, Daniel Vallicotti, and Stephan Teichtmeister. Homogenization and multiscale stability analysis in finite magneto-electro-elasticity. application to soft matter ee, me and mee composites. *Computer Methods in Applied Mechanics and Engineering*, 300:294–346, 2016.

[67] Erato Psarra, Laurence Bodelot, and Kostas Danas. Two-field surface pattern control via marginally stable magnetorheological elastomers. *Soft Matter*, 13:6576–6584, 2017.

[68] Mokarram Hossain, Duc Khoi Vu, and Paul Steinmann. Experimental study and numerical modelling of vhb 4910 polymer. *Computational Materials Science*, 59:65–74, 2012.

[69] Ashkan Dargahi, Ramin Sedaghati, and Subhash Rakheja. On the properties of magnetorhe-

ological elastomers in shear mode: Design, fabrication and characterization. *Composites Part B: Engineering*, 159:269–283, 2019.

[70] Hossein Vatandoost, Masoud Hemmatian, Ramin Sedaghati, and Subhash Rakheja. Dynamic characterization of isotropic and anisotropic magnetorheological elastomers in the oscillatory squeeze mode superimposed on large static pre-strain. *Composites Part B: Engineering*, 182:107648, 2020.

[71] Ioan Bica, Eugen M. Anitas, Larisa Marina Elisabeth Averis, Seung Hyuk Kwon, and Hyoung Jin Choi. Magnetostrictive and viscoelastic characteristics of polyurethane-based magnetorheological elastomer. *Journal of Industrial and Engineering Chemistry*, 73:128–133, 2019.

[72] Anna Boczkowska and Stefan Awietjan. Microstructure and properties of magnetorheological elastomers. In Anna Boczkowska, editor, *Advanced Elastomers*, chapter 6. IntechOpen, Rijeka, 2012.

[73] Dirk Romeis, Vladimir Toshchevikov, and Marina Saphiannikova. Effects of local rearrangement of magnetic particles on deformation in magneto-sensitive elastomers. *Soft Matter*, 15:3552–3564, 2019.

[74] Karl A. Kalina, Philipp Metsch, Jörg Brummund, and Markus Kästner. A macroscopic model for magnetorheological elastomers based on microscopic simulations. *International Journal of Solids and Structures*, 193-194:200–212, 2020.

[75] Guojiang Liao, Xinglong Gong, Shouhu Xuan, Chaoyang Guo, and Luhang Zong. Magnetic-field-induced normal force of magnetorheological elastomer under compression status. *Industrial & Engineering Chemistry Research*, 51(8):3322–3328, 2012.

[76] Dmytro Ivaneyko, Vladimir Toshchevikov, Marina Saphiannikova, and Gert Heinrich. Mechanical properties of magneto-sensitive elastomers: unification of the continuum-mechanics and microscopic theoretical approaches. *Soft Matter*, 10:2213–2225, 2014.

[77] Wei Gao and Xingzhe Wang. Experimental and theoretical investigations on magnetoelastic

shear behavior of isotropic mr elastomers under gradient magnetic fields. *Journal of Magnetism and Magnetic Materials*, 483:196–204, 2019.

[78] B X Ju, M Yu, J Fu, Q Yang, X Q Liu, and X Zheng. A novel porous magnetorheological elastomer: preparation and evaluation. *Smart Materials and Structures*, 21(3):035001, feb 2012.

[79] O. Biro and K. Preis. On the use of the magnetic vector potential in the finite-element analysis of three-dimensional eddy currents. *IEEE Transactions on Magnetics*, 25(4):3145–3159, 1989.

[80] Heng Wu, Zhiqiang Xu, Jun Wang, Xinqian Bo, Zhifa Tang, Shengqiang Jiang, and Gaofeng Zhang. Chain formation mechanism of magnetic particles in magnetorheological elastomers during pre-structure. *Journal of Magnetism and Magnetic Materials*, 527:167693, 2021.

[81] Y. Gao, M. A. Hulsen, T. G. Kang, and J. M. J. den Toonder. Numerical and experimental study of a rotating magnetic particle chain in a viscous fluid. *Phys. Rev. E*, 86:041503, Oct 2012.

[82] Maarten M. van Oene, Laura E. Dickinson, Francesco Pedaci, Mariana Köber, David Dulin, Jan Lipfert, and Nynke H. Dekker. Biological magnetometry: Torque on superparamagnetic beads in magnetic fields. *Phys. Rev. Lett.*, 114:218301, May 2015.

[83] Randall M. Erb, Joshua J. Martin, Rasam Soheilian, Chunzhou Pan, and Jabulani R. Barber. Actuating soft matter with magnetic torque. *Advanced Functional Materials*, 26(22):3859–3880, 2016.